Chapter – III

Geochemical evolution of the Neoproterozoic – early Cambrian Marwar Basin

3.1 Introduction

The Neoproterozoic Era (1000 - 541 Ma) had witnessed dynamic changes in climate in the form of three global glaciations (Halverson and Shields-Zhou, 2011; Hoffman et al., 1998), biological evolution with the emergence and the subsequent extinction of Ediacaran fauna (Canfield et al., 2007; McFadden et al., 2008), and tectonics in terms of continental configurations (Collins and Pisarevsky, 2005; Meert, 2003). Also, the period has seen an enigmatic negative excursion in the marine carbonate record globally known as the Shuram anomaly where the $\delta^{13}C$ drops to ~-12‰ (Grotzinger et al., 2011). The supercontinent Rodinia broke apart and the stage was set for the amalgamation of Gondwanaland (Li et al., 2008).

Deposition of the Marwar Supergroup of Rajasthan, western India took place during this Era. Sedimentation in the basin possibly started subsequent to the break-up of Rodinia (Roy and Jakhar, 2002) and believed to have continued through the period that saw the formation of Gondwanaland (McKenzie et al., 2011), thus making it contemporaneous with the Huqf Supergroup of Oman, Salt Range of Pakistan, Krol-Tal Groups of the Himalaya and Molo Group of Madagascar (Cozzi et al., 2012; Davis et al., 2014; Turner et al., 2014). Paleomagnetic studies within the Marwar Supergroup suggest an equatorial paleogeographic position for the Indian shield during basin development alongside the Arabian-Nubian shield, Eastern Antarctica and Australia in the Ediacaran-early Cambrian Period (Davis et al., 2014). However, an intermediate northerly latitude is also proposed for the basement of the basin; the ~750 Ma old Malani Igneous Suite (MIS), which suggests that the Indian shield along with Laurentia, Baltica, South China and Seychelles formed the western margin of the Rodinia (Gregory et al., 2009; Meert et al., 2013; Torsvik et al., 2001). Furthermore, there have been growing support for the view, from various microbially induced sedimentary structures (MISS) (Kumar and Ahmad, 2014; Sarkar et al., 2008) and Edicaran-type fossils (Kumar et al., 2009) within the lower part of the Marwar Supergroup, that the sedimentation in the basin started well before the Ediacaran Period. Deposited in a shallow intracratonic sag basin, the Marwar Supergroup consists of largely unmetamorphosed and undeformed fluvial and marginal marine siliciclastics, marine carbonates and minor volcaniclastics (Paliwal, 1998; Pareek, 1981; Roy and Jakhar, 2002). Because of its temporal occurrence and likely spatial configuration, the basin and its sedimentary record hold keys to our understanding of the post-Rodinian tectono-climatic evolution of the Indian shield.

3.2 Objectives

The specific objectives of the present work were to,

1. Look for chemical signatures, particularly in the $\delta^{13}C$ record, of the three Neoproterozoic global glaciations and the Shuram $\delta^{13}C$ anomaly in the carbonate formations of the Marwar Supergroup.

2. Establish the chronology of events by providing age constraints on deposition of various formations using Rb-Sr isochron dating of a tuff layer in the lower Marwars and $^{87}Sr/^{86}Sr$ stratigraphy of the carbonate sequences.

3. Decipher the sedimentary history of the basin by constraining the provenance of the siliciclastic formations and siliciclastics within the carbonate formations of the Supergroup using variations in trace element contents and radiogenic isotopic (Sr-Nd) compositions as proxies.

3.3 Geological setting

3.3.1 Regional geology

The Aravalli Craton is generally considered to be represented by the 3.3 – 2.5 Ga Banded Gneissic Complex (BGC-1) in southern Rajasthan which forms the basement of subsequent magmatic activities and sedimentary deposits (Fig. 3.1; Gopalan et al., 1990; Roy and Kröner, 1996; Wiedenbeck and Goswami, 1994). It consists dominantly of amphibolite to granulite grade tonalitic and granodioritic gneisses, with associated lenticular masses of amphibolite. The ancestry of the BGC of central Rajasthan (BGC-2), however, remains equivocal (Fig. 3.1;

Bhowmik and Dasgupta, 2012; Buick et al., 2006; Tobisch et al., 1994). This slightly younger basement is exposed to the north of the BGC-1. It is subdivided into 1) the Sandmata Complex consisting of granulites and 2) the Mangalwar Complex; a spatially more extensive assemblage of gneisses, meta-granitoids and minor amphibolites. The stabilization of the Aravalli Craton at ~2.5 Ga (Wiedenbeck et al., 1996) was followed by sedimentation of the Aravalli Supergroup (2.3 – 1.6 Ga ?) and the Delhi Supergroup (1.8 – 0.8 Ga ?; Ahmad et al., 2008; Biju-Sekhar et al., 2003; Kaur et al., 2011b; McKenzie et al., 2013; Van Lente et al., 2009). A major thermal event is believed to have occurred in the Aravalli Craton at ~1.7 Ga and is manifested in most of the geochronological data reported from the region (Buick et al., 2006; Roy et al., 2005; Tobisch et al., 1994). The Delhi Supergroup is intruded by numerous granitic plutons that largely fall into two categories; 1) the older 1.7 - 1.8 Ga group, which is exposed mostly in the northeastern part of the Delhi Fold Belt (DFB; Biju-Sekhar et al., 2003; Choudhary, 1984; Kaur et al., 2011a, 2009, 2007) and 2) the younger (0.8 – 1.0 Ga) and abundant group of rocks known as the Erinpura Granites that are exposed in the southwestern part (Choudhary, 1984; Pandit et al., 2003; Van Lente et al., 2009). A metasedimentary sequence, known as the Sirohi Group, comprising of shales and carbonates metamorphosed to lower greenschist facies, is exposed within the younger DFB granitoids (Purohit et al., 2012). The Precambrian magmatic activity in the Aravalli Craton ended with the voluminous 770-750 Ma Malani magmatism, which produced a suite of rocks that are dominated by rhyolites with minor basic volcanics and granitoids (Crawford and Compston, 1970; Gregory et al., 2009; Meert et al., 2013; Rathore et al., 1999).

3.3.2 The Marwar Supergroup

The Marwar Supergroup unconformably overlies the MIS, covering an area of over 100,000 km^2 (Kumar, 1999; Fig. 3.1). The Aravalli Mountain range, the Delhi-Lahore subsurface ridge and the Devikot-Nachna subsurface high form the boundaries of the basin in east, north and southwest, respectively (Pareek 1984; 1981). Most of the north and northeastern parts of the basin are covered by the Quaternary sand deposits. The MIS forms the basement of the Marwar basin in central and western regions. The eastern Marwars are exposed near the Khatu village and are deposited over a sequence of highly deformed metasediments, which belongs to the ~850 Ma old Sirohi Group (Paliwal, 1998). The Erinpura Granites also form the basement of the basin in certain parts of the eastern fringes (Linnemann and Sharma, 2014). The Marwar Supergroup has a maximum thickness of 2000 m (Pareek, 1981) and is classified into three groups from bottom to top as: the Jodhpur Group, the Bilara Group and the Nagaur Group (Fig. 3.2). At the western margin of the basin, the unconformity between the MIS and the Marwar Supergroup is represented by the Pokaran Boulder Bed (Fig. 3.2). The origin and chronology of this boulder bed remain uncertain with some believing it to be of glacial origin (Chauhan et al., 2001) and others argue for a fluvial origin (Cozzi et al., 2012).

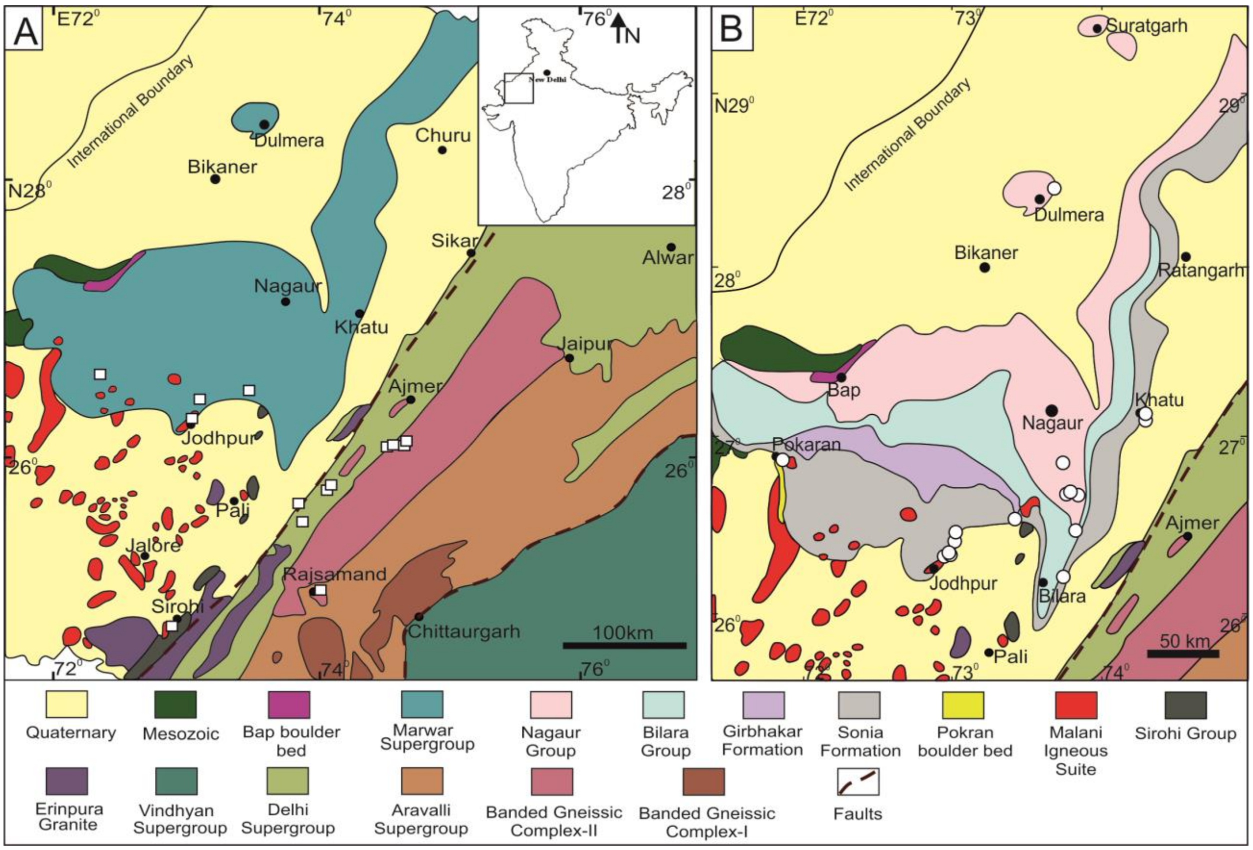

Figure 3.1: (A) Geological map of western India showing the Marwar Supergroup and surrounding litho-tectonic units (modified after Roy and Jakhar, 2002). The study area is marked in the inset and sampling locations of the basement rocks are shown as white squares. (B) Geological map of the Marwar Supergroup with stratigraphic subdivisions (modified after Pareek, 1984). Locations of the samples from Marwar Supergroup are shown as white circles.

The overlying Sonia Formation consists of red and white sandstones and maroon shales, all believed to have formed in deltaic and beach environment (Chauhan et al., 2004). The formation also has a dolostone member exposed at Artiya Kalan, near Jodhpur. The top part of the Jodhpur Group, the Girbhakar Formation is a gritty and pebbly sandstone of fluvial origin (Chauhan et al., 2004). Paliwal (1998) reported occurrences of felsic volcanics; rhyolites and alternate layers of calcareous tuff and pure ash beds sandwiched between the Sonia and Girbhakar Formations, within the Jodhpur Group in the eastern part of the basin at Chhoti Khatu village (Figs. 3.2 and 3.3). The calcareous tuff consists of angular fragments of quartz, K-feldspar, randomly oriented blades of biotite and muscovite, minor chert and glass shards in a siliceous-micritic groundmass (Fig. 3.3C). Volcanic debris trapped in microbialite lamellae and angular fragments of pure rhyolite are also present in the tuff. The shallow marine carbonate rocks of the Bilara Group form the middle portion of the Marwar Supergroup. It is divided, from bottom to top, into three formations: 1) The Dhanapa Formation which consists of stromatolitic dolostone, 2) the Gotan Formation that contains wavy, laminated limestone, and 3) the Pondlo Formation made entirely up of dolostone. The Bilara Group also includes subsurface evaporites (Das Gupta, 1996) which are considered to be a facies variation of the carbonates (Mazumdar and Bhattacharya, 2004; Mazumdar and Strauss, 2006). The Nagaur Group, which includes the Nagaur and Tunklian Formations, consists of braided fine to coarse grained reddish brown sandstones and siltstones of fluvial origin (Pareek, 1981). They are unconformably overlain by the Permo-Carboniferous Bap Boulder Bed (Pandey and Bahadur, 2009).

3.3.3 Chronology of sedimentation

The Marwar Supergroup has been traditionally considered to be Neoproterozoic in age (Pandit et al., 2001). However, there were no radiometric dates available to constrain ages of deposition of various formations. The terminal dyke phase of the basement MIS has been dated to 752±18 (2σ) Ma (Fig. 3.2; Meert et al., 2013). This forms the lower time bound of the Marwar Supergroup. The current understanding of the antiquity of deposition of various groups in the basin is primarily based on biostratigraphy. Body fossils like *Hiemalora*, *Aspidella*, *Beltanelliformis minuta* (Kumar and Pandey, 2009; Raghav et al., 2005) and various microbially induced sedimentary structures (MISS) have been reported from the Jodhpur Group (Kumar and Ahmad, 2014; Kumar and Pandey, 2009; Sarkar et al., 2008) suggesting a Late Neoproterozoic sedimentation for the lower Marwars. Kumar and Pandey (2010) reported Cambrian trace fossils like *Rusophychus* and *Cruziana* from the lower part of the Nagaur Formation indicating that the Marwar sedimentation extended well into the Cambrian. Using Sr isotope stratigraphy of carbonates, Mazumdar and Strauss (2006) suggested that the Bilara Group ($^{87}Sr/^{86}Sr$=0.7082) was deposited during the Ediacaran to early Cambrian time. The detrital zircon age data from the sandstones of the Jodhpur Group show the youngest peak at ~750 Ma, which is essentially the age of the basement MIS and the older age peaks of ~850 Ma and ~1.8 Ga are likely from the Erinpura and BGC-2, respectively (Malone et al., 2008; Turner et al., 2014). McKenzie et al. (2011) carried out detrital zircon analysis of the Naguar Formation and reported youngest mode of zircon ages at ~540 Ma, which can be considered as the maximum age of the Nagaur Formation (Fig. 3.2).

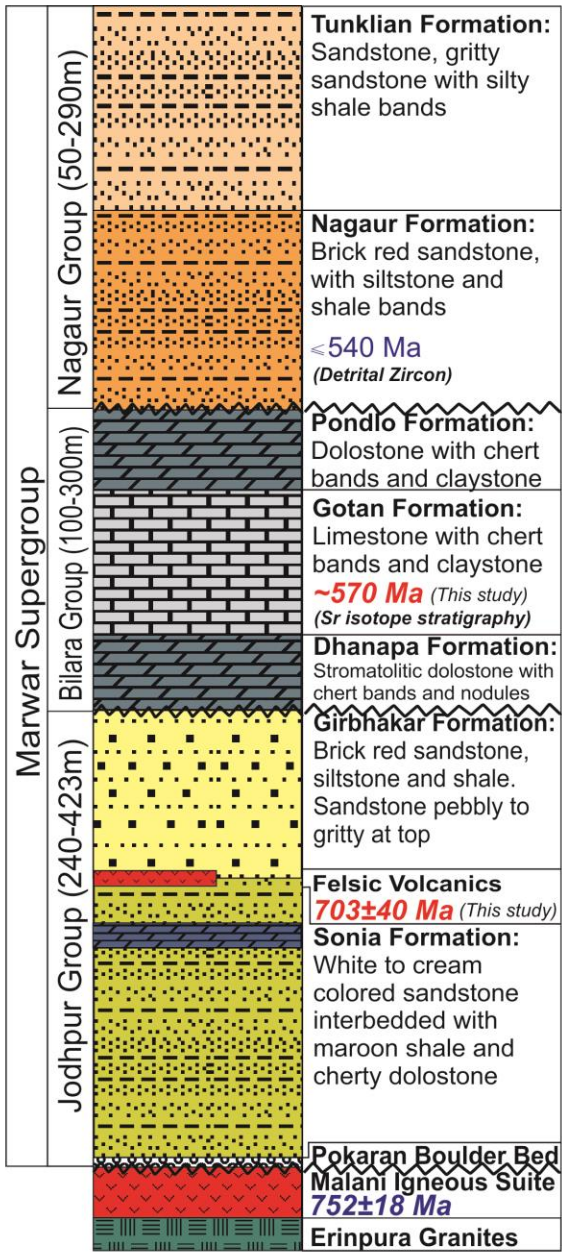

Figure 3.2: Simplified stratigraphy of the Marwar Supergroup based on information given in Pareek, (1984). Age constraints are from McKenzie et al., (2011); Meert et al., (2013) and the present study. Errors in the ages are 2σ.

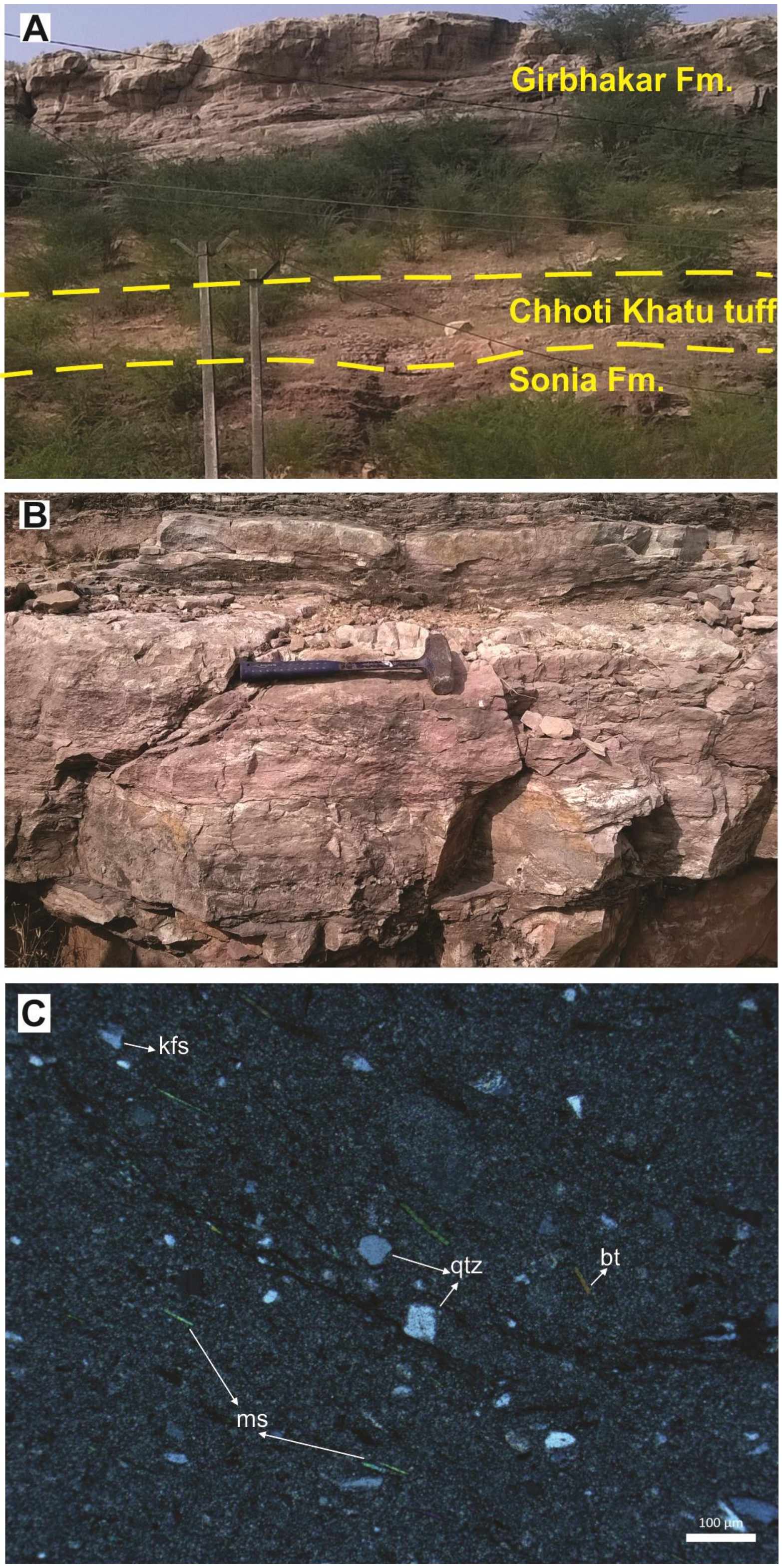

Figure 3.3: (A) Outcrop photo of the calcareous tuff at Chhoti Khatu village, eastern Marwars. (B) A close up outcrop photo of the tuff layer. (C) Photomicrograph of the calcareous tuff under cross polarized transmitted light showing angular fragments of quartz and feldspar, blades of mica in a siliceous-micritic groundmass.

3.4 Samples and methods

We carried out extensive field work and sampling of siliciclastic sedimentary rocks, carbonates and volcaniclastics from various parts of the Marwar basin. Locations and a brief descriptions of the samples used in the present study are given in Table 3.1. Siliciclastics were sampled in and around Jodhpur, Nagaur, and Dulmera. Carbonate formations of the Bilara Group were sampled from various limestone mines located at Bilara, Gotan, and Khimsar towns, whereas the dolostone member of the Sonia Formation was sampled at Artiya Kalan village near Jodhpur. The Chhoti Khatu Tuff was sampled near the Khatu village. Samples were also collected from the potential source regions of sediments. This includes samples of BGC-2, Delhi and Aravalli Supergroups collected near Beawar, Phulad and Udaipur localities, respectively. The Erinpura Granites and MIS were sampled near Sirohi and Jodhpur towns. A brief account of the sample preparation protocols and various analytical techniques employed is given in Chapter – 2, and will not be discussed here.

3.5 Results

3.5.1 Geochronology

Rb-Sr whole rock isotopic ratio and concentration data of the Chhoti Khatu tuff are given in Table 3.2. The Rb-Sr whole-rock isochron is plotted in Fig. 3.4A, with the linear regression fitted using Isoplot 3.75 (Ludwig, 2012) yielding a date of 703±40 Ma (2σ; MSWD=2.3). The regression line is not a mixing line because the initial $^{87}Sr/^{86}Sr$ remains constant when plotted against the varying 1/Sr (Fig. 3.4B), which suggests that the silicate materials in the tuff were derived from a (isotopically) homogenized magma. Mixing, if any, could have happened at the source giving a crustal signature to the initial ratio ($^{87}Sr/^{86}Sr_{init}$ = 0.7605). Therefore, the date of 703 Ma can be considered as the age of crystallization of the minerals in the tuff, and hence, the age of deposition of the formation. Although, the Rb-Sr dating method is not as robust as the U-Pb zircon dating, the fact that a previous attempt using the latter could only provide a maximum age of ~700 Ma (the age of the youngest recycled zircon; Xu and Meert, 2014) makes our Rb-Sr isochron age significant.

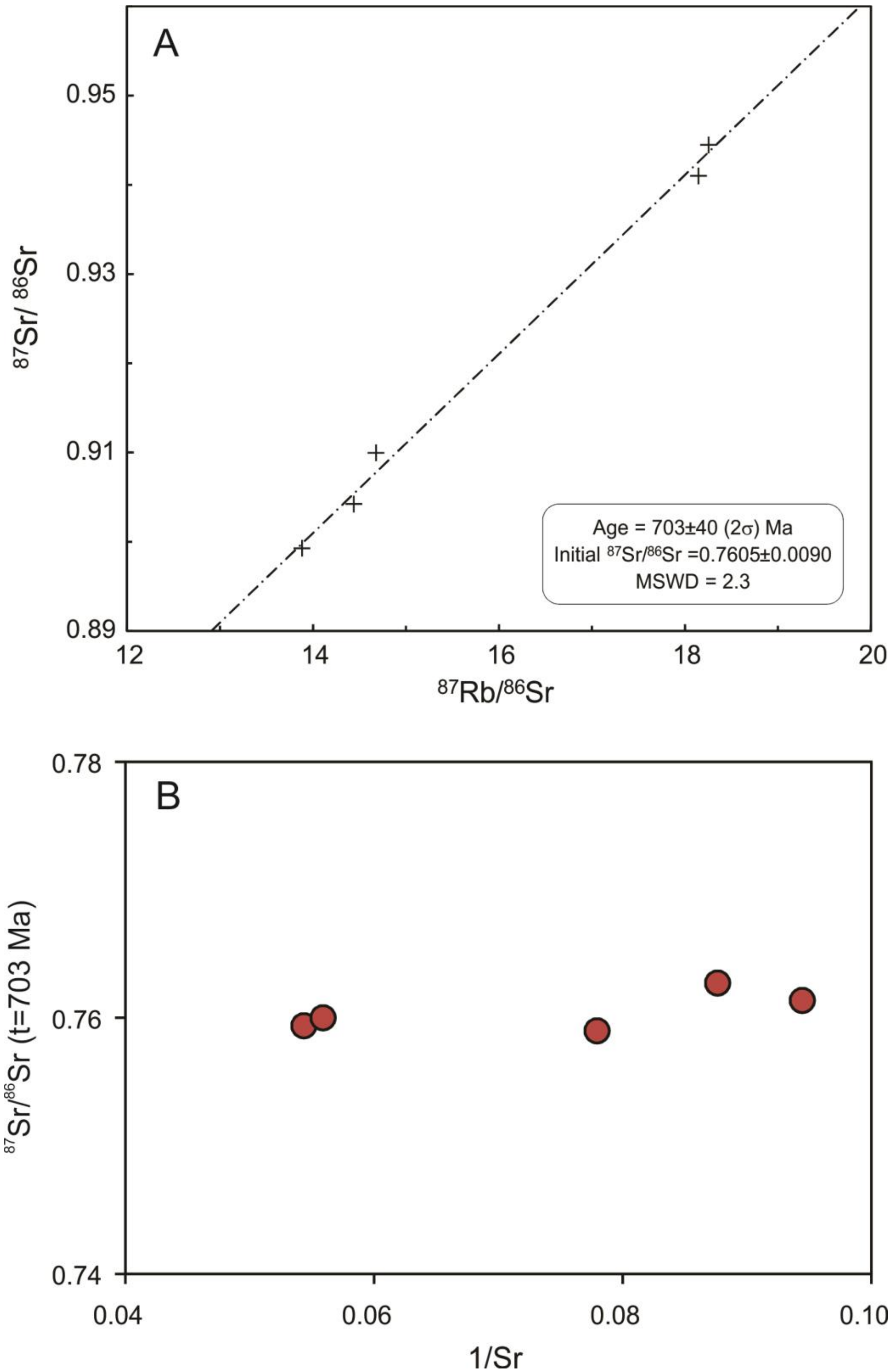

Figure 3.4: (A) Plot of $^{87}Sr/^{86}Sr$ versus $^{87}Rb/^{86}Sr$ for Chhoti Khatu Tuff using data from Table 1. The isochron and age calculations are done using Isoplot 3.75 (Ludwig, 2012). Uniform errors of 1.5% and 0.001% for $^{87}Rb/^{86}Sr$ and $^{87}Sr/^{86}Sr$, respectively, are used for the isochron. (B) Plot of $^{87}Sr/^{86}Sr$ (t=703 Ma) versus 1/Sr for Chhoti Khatu Tuff.

3.5.2 $^{87}Sr/^{86}Sr$ isotope stratigraphy

The Sr isotopic composition of the seawater is controlled by two sources – the hydrothermal input and the continental run-off (Faure, 1986). Sr from the seawater substitutes for Ca in the marine carbonates, thereby leaving them with the $^{87}Sr/^{86}Sr$ of the seawater from which they were precipitated. However, the primary $^{87}Sr/^{86}Sr$ of the carbonates can at times be altered by the secondary meteoric fluids with highly radiogenic $^{87}Sr/^{86}Sr$, changing their pristine $^{87}Sr/^{86}Sr$ to more radiogenic values. The Sr isotopic composition and the trace element data of the carbonate formations of the Marwar Supergroup are presented in Table 3.3. The dolostone member of the bottommost Sonia Formation displays $^{87}Sr/^{86}Sr$ from 0.7169 to 0.7199. These ratios are higher than the highest observed $^{87}Sr/^{86}Sr$ values of the seawater during its evolution indicating that these are altered and therefore cannot be used for Sr isotope stratigraphy (Shields and Veizer, 2002). The single sample from the stromatolitic Dhanapa Dolostone of the overlying Bilara Group possesses $^{87}Sr/^{86}Sr = 0.7092$. Although the sample shows low Mn/Sr (Mn/Sr = 1.2), better than the empirical ratio of 1.5 below which the Sr isotope system is generally considered unaltered in carbonates (Knoll et al., 1995), its $^{87}Sr/^{86}Sr$ are radiogenic than the seawater $^{87}Sr/^{86}Sr$ reported during late Neoproterozoic and early Cambrian indicating that the sample did not preserve its original composition and cannot be used for constraining the age of deposition of the Dhanapa Dolostone.

The $^{87}Sr/^{86}Sr$ of the Gotan Limestone varies from 0.7081 to 0.7110 and Mn/Sr from 0.03 to 5.3. However, a majority of the samples has Mn/Sr <1 and Mg/Ca <0.1 (Table 3.3), suggesting least altered nature of their Sr systematics, and therefore, such samples were selected for Sr isotope stratigraphy. To determine the most pristine $^{87}Sr/^{86}Sr$ of the Gotan Formation that could represent the seawater from which it precipitated, we plotted $^{87}Sr/^{86}Sr$ vs. Ca/Sr (Fig. 3.6D). The plot yielded a linear relationship with the sample showing the lowest $^{87}Sr/^{86}Sr$ also has the highest Sr content and Mn/Sr of 0.14. This ratio (0.708097) can be considered as the best representative of the primordial $^{87}Sr/^{86}Sr$ for the formation and thus the ratio in the coeval seawater. The ratio yielded two probable ages; an early Cambrian age of 520-530 Ma and a late Edaicaran age of ~570 Ma, when correlated with the global seawater Sr isotope curve (McArthur et al., 2012). However, the detrital zircon maximum age constraint of 540 Ma placed on the overlying Nagaur Formation (McKenzie et al., 2011) and lack of evidence for any Cambrian fossils in the Gotan Formation hints at a late Ediacaran age (~570 Ma) for the Gotan Formation. It should be noted that this is an approximate age because the method is a relative dating technique and the uncertainty, associated with fitting of the seawater evolution curve for $^{87}Sr/^{86}Sr$ from which ages are determined, is large (≥50Ma).

$^{87}Sr/^{86}Sr$ of the overlying Pondlo Dolostone ranges from 0.7088 to 0.7102, their Mn/Sr varies from 0.4 to 80, and Mg/Ca varies from 0.003 to 1.1 (Table 3.3). The lowest $^{87}Sr/^{86}Sr$ of the formation, 0.7088, is higher than the reported seawater ratios of the late Neoproterozoic and early Cambrian suggesting that the Sr systematics of the formation is altered and, therefore cannot be used for constraining the age of the formation.

3.5.3 Stable C and O isotope geochemistry

The carbon and oxygen isotopic compositions of the carbonate formations of the Marwar Supergroup are presented in Table 3.3. The carbon isotopic composition of the carbonate samples is largely resilient to post-depositional alteration because of buffering effect and hence is considered to represent the composition of the contemporary seawater from which they were precipitated. However, if the diagenetic fluid is charged with CO_2 then there is possibility that the primary signals of $\delta^{13}C$ may get altered. Therefore, we have utilized $\delta^{18}O$ and various other trace and major element ratios, such as Mn/Sr, Ca/Sr, and Mg/Ca, to evaluate the extent of modification (if any) of the primary $\delta^{13}C$ signals of the samples.

The $\delta^{13}C$ of the dolostone member within the Sonia Formation vary between -4.7 and 2.4‰, and the $\delta^{18}O$ between -9.7 and 0‰ (Fig. 3.5). All the dolostone samples (Mg/Ca ≥ 0.4) show $\delta^{18}O$ > -10‰, an empirically constrained value above which $\delta^{13}C$ of the carbonates is generally considered unaltered (Knoll et al., 1995). However, such high $\delta^{18}O$ need not always be primary in nature since dolomitization in an evaporative environment could also result in high $\delta^{18}O$ (Kah, 2000). Additionally, the samples display very high Mn/Sr, between 59 and 126, much above the empirical value of 10, beyond which $\delta^{13}C$ of the formation is considered altered and may not represent the $\delta^{13}C$ of the contemporary seawater (Knoll et al., 1995). Hence, the $\delta^{13}C$ values from the dolostone member will not be used by me further in the interpretations as they do not truly reflect the $\delta^{13}C$ of the contemporary seawater.

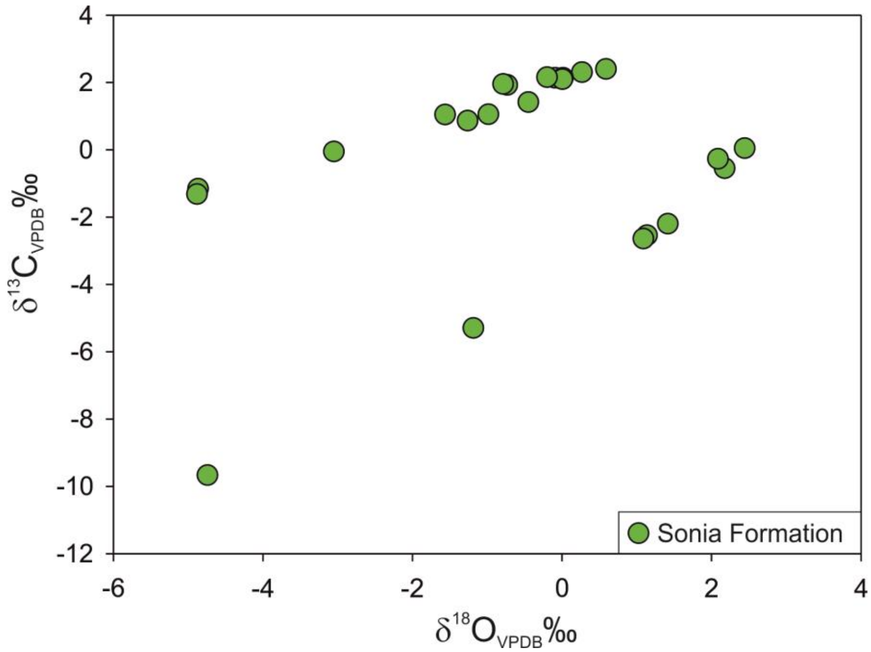

Figure 3.5: Plot of $\delta^{13}C$ vs. $\delta^{18}O$ for samples from the dolostone member of the Sonia Formation

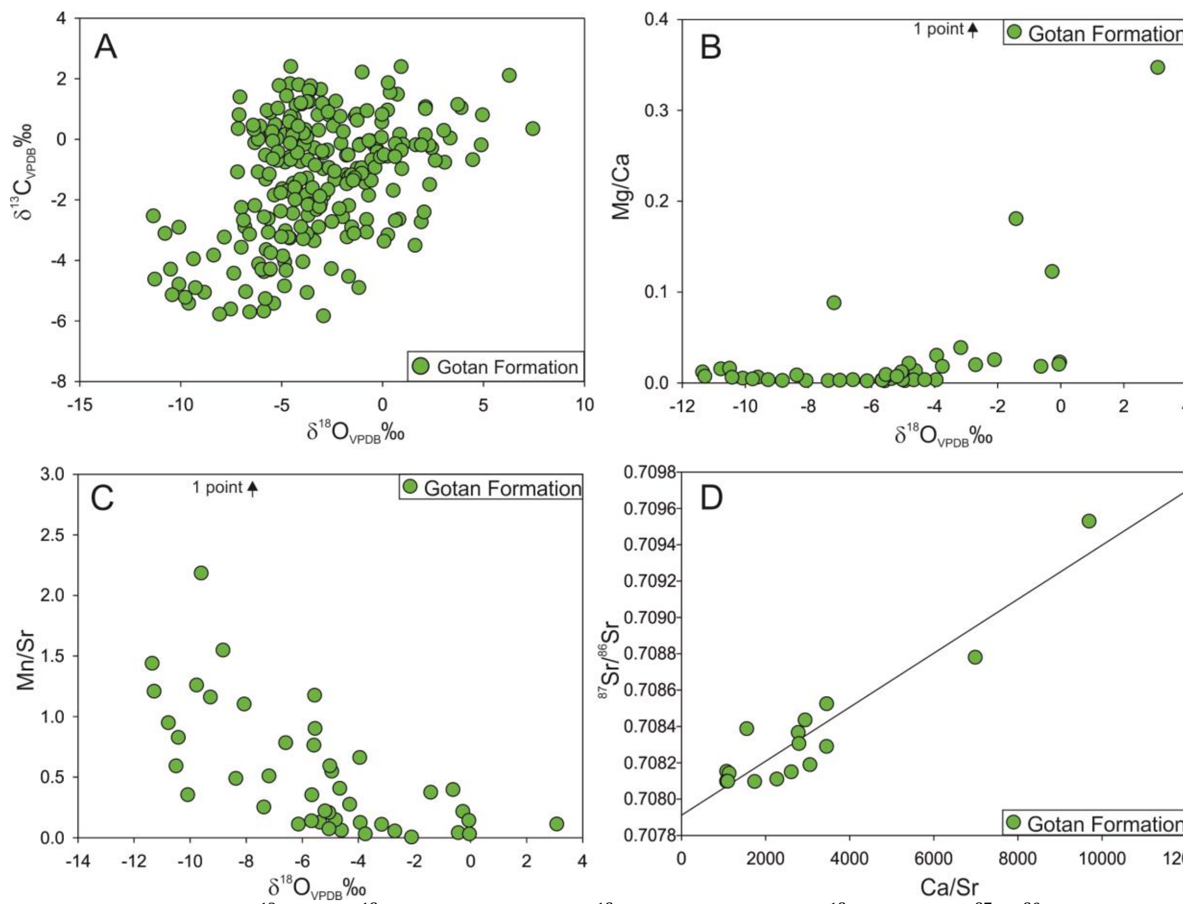

Figure 3.6: Plots of $\delta^{13}C$ vs. $\delta^{18}O$ (A), Mg/Ca vs. $\delta^{18}O$ (B), Mn/Sr vs. $\delta^{18}O$ (C), and $^{87}Sr/^{86}Sr$ vs. Ca/Sr (D) for samples from the Gotan Limestone.

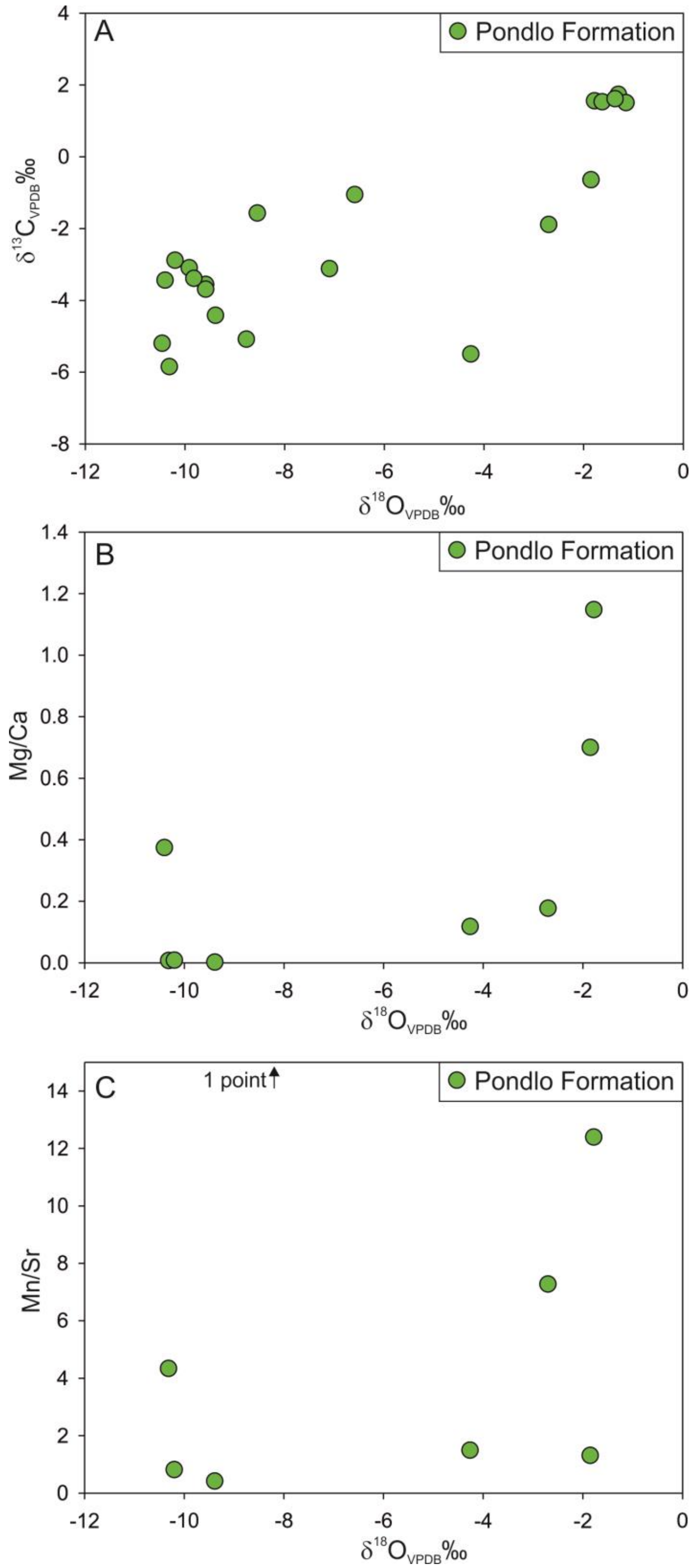

Figure 3.7: Plots of $\delta^{13}C$ vs. $\delta^{18}O$ (A), Mg/Ca vs. $\delta^{18}O$ (B), and Mn/Sr vs. $\delta^{18}O$ (C) for samples from the Pondlo Dolostone.

The single dolostone sample (Mg/Ca = 1.2) from the Dhanapa Formation displays $\delta^{13}C$ of -1.9‰ and $\delta^{18}O$ of -2.1‰, respectively (Table 3.3). The high $\delta^{18}O$ and low Mn/Sr (Mn/Sr = 1.2) suggest dolostone formation could have preserved its primordial $\delta^{13}C$ signals. The $\delta^{13}C$ and $\delta^{18}O$ of the Gotan Limestone range from -5.7 to 2.4‰ and -11.4 to 7.4‰, whereas the overlying Pondlo Dolostone display $\delta^{13}C$ and $\delta^{18}O$ from -5.8 to 1.6‰ and -10.5 to -1.2‰, respectively (Figs. 3.6A and 3.7A). The Mn/Sr of the Gotan Limestone ranges from 0.03 to 5.3 (Fig. 3.6C). Nonetheless, majority of the Gotan samples show Mn/Sr < 1 and $\delta^{18}O$ > -10‰, indicating that the samples most likely have preserved the primordial $\delta^{13}C$. The Pondlo Dolostone shows a large variation in the Mn/Sr with values ranging from 0.4 to 80 (Fig. 3.7C); however, majority of the samples show Mn/Sr < 10 and $\delta^{18}O$ > -10 suggesting the formation too have retained its initial $\delta^{13}C$.

3.5.4 Trace element geochemistry

Trace element data for siliciclastic sediments of the Marwar Supergroup are presented in Table 3.4 and are plotted in Fig. 3.8. In the Primitive Mantle (PM) normalized diagram (Fig. 3.8A) these sediments generally show enrichments in Th, U and Pb and depletions in Nb, Ta, Sr and Eu. They also show LREE enriched patterns in the Chondrite normalized plot (Fig. 3.8B), with the La_N/Yb_N ranging from 4.7 to 27.4. HREE show almost flat patterns (Fig. 3.8B), with Gd_N/Yb_N falling in a range of 1.0 to 3.5. A conspicuous negative Eu anomaly is observed in all samples (Fig. 3.8B) with an average [Eu/Eu*] value of 0.64.

Among the basement rocks we have analyzed (Table 3.5); the Malani rhyolites show a noticeable depletion in Sr and Eu when compared with the Marwar sedimentary rocks in the PM normalized plot (Fig. 3.8A). The basement at the eastern parts of the basin, the Erinpura Granites, shows similar patterns as that of the Marwar sediments albeit with depletions in Zr and Hf. All the probable source rocks show LREE enriched Chondrite normalized patterns (not shown). The La_N/Yb_N ranges from 3.5 to 5.3 for the Malani rhyolite and 2.3 to 10.9 for the Erinpura Granites. The gneiss samples from BGC-2 show higher values for La_N/Yb_N ratio ranging from 10.4 to 18.1, while rocks from the Delhi Supergroup have this ratio in the range of 1.8 to 16.4. The Gd_N/Yb_N ratio ranges from 1.1 to 1.7 in the Malani Rhyolite, 0.9 to 2.1 in the Erinpura Granites, 1.7 to 3.9 in the BGC-2 and 1.0 to 2.9 in the Delhi Supergroup.

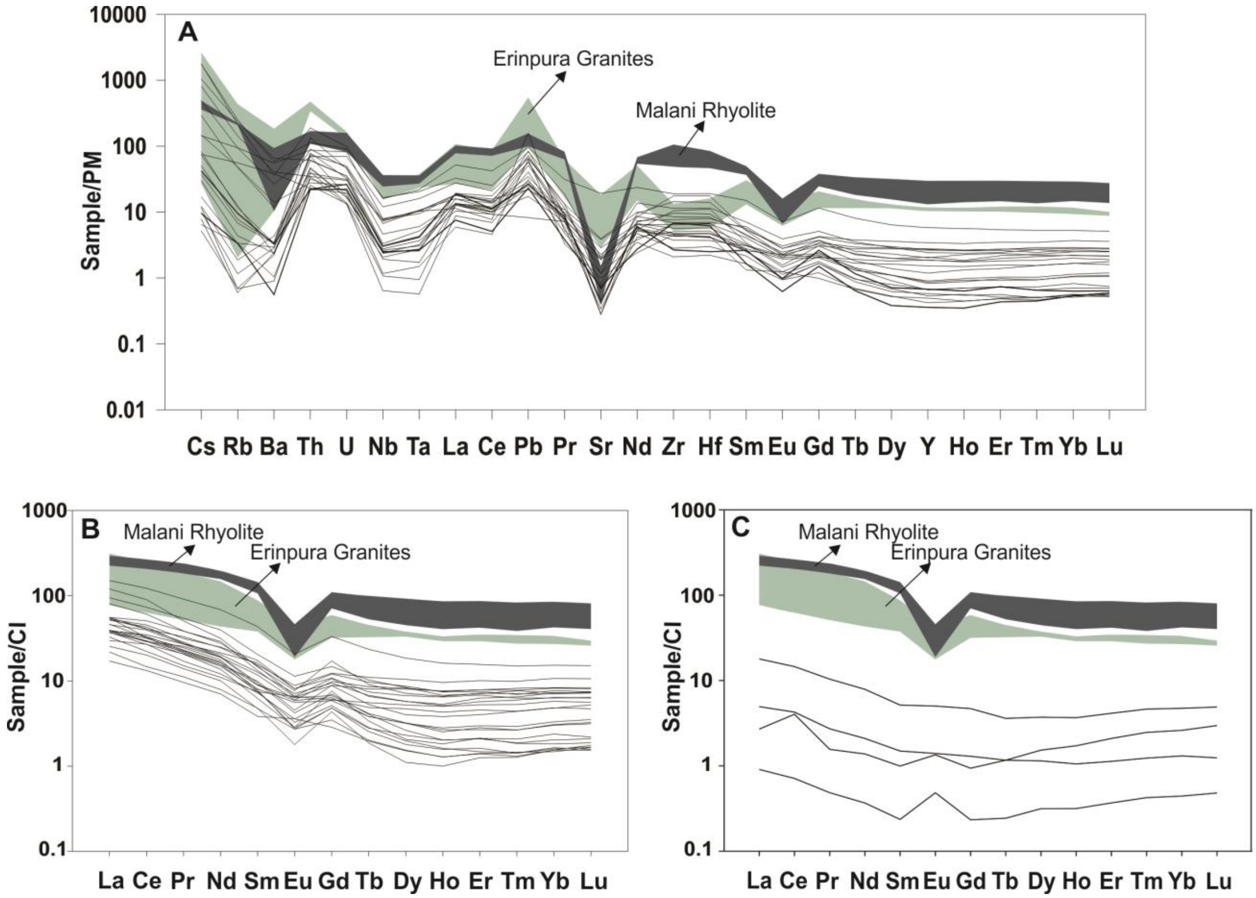

Figure 3.8: Primitive Mantle normalized multi-element (A) and Chondrite normalized rare earth element (REE) (B) patterns for samples from the siliciclastic formations of the Marwar Supergroup. (C) Chondrite normalized REE patterns for silicate fractions of the samples from the Gotan Limestone. Patterns for basement rocks (MIS rhyolites and Erinpura Granites) are given for comparison. The CI Chondrite and Primitive Mantle values are from Sun and McDonough, (1989).

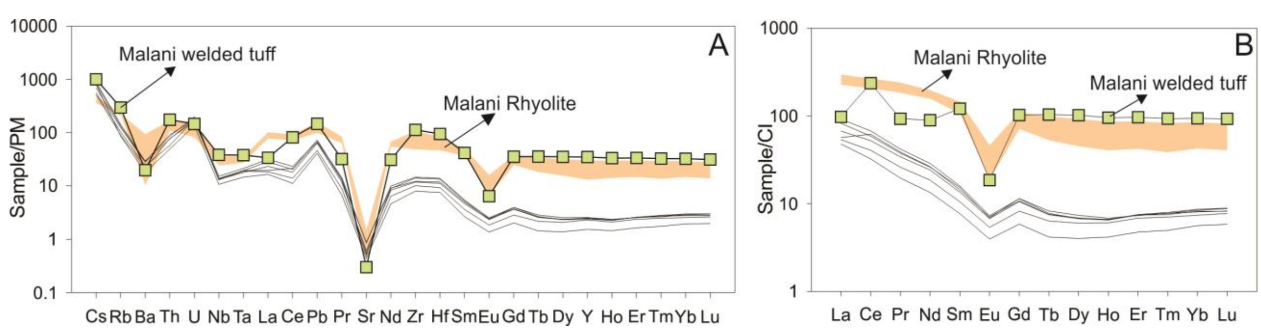

Figure 3.9: (A) Primitive Mantle normalized multi-element, and (B) Chondrite normalized rare earth element (REE) patterns for samples from the Chhoti Khatu Tuff. Data for the Malani Rhyolites and welded tuff are plotted for comparison. The CI Chondrite and Primitive Mantle values are from Sun and McDonough, (1989).

Trace element data of the Chhoti Khatu Tuff are presented in Table 3.4 and are plotted in Fig. 3.9. In the Primitive Mantle normalized diagram, the tuff samples show depletions in Sr, Eu, Nb, Ta, and enrichment in Pb. They exhibit LREE enriched patterns in the Chondrite normalized plot, with La_N/Yb_N ratio ranging from 6.6 to 10.9, and relatively flat HREE patterns with an average Gd_N/Yb_N = 1.2, The tuff samples show a conspicuous negative Eu anomaly with an average [Eu/Eu*] = 0.56.

3.5.5 Sr-Nd isotope geochemistry

The Sr and Nd isotopic ratio data for all the samples are given in Table 3.4. The $^{87}Sr/^{86}Sr$ of the sandstone samples from the Jodhpur Group vary in the range of 0.71 – 0.79 and that of the intercalated shale bands in the range of 0.72 – 0.87 (Table 3.4). Nagaur Group rocks display a larger spread in their $^{87}Sr/^{86}Sr$ values: 0.72 – 0.84. All the samples display predominantly crustal signatures. However, considering that $^{87}Sr/^{86}Sr$ is heavily dependent on grain size variation and susceptible to alteration by secondary processes (e.g., diagenesis and metamorphism) we use it sparingly for our interpretations on the provenances. The Chhoti Khatu Tuff displays highly radiogenic $^{87}Sr/^{86}Sr$ varying from 0.8993 to 0.9445.

The ε_{Nd} (0) of Marwar siliciclastic sediments vary from -21.8 to -8.5 (Table 3.4). ε_{Nd} (0) of the Sonia Sandstone at the contact with basement shows an average value of -9.0, whereas the middle and upper parts of the formation have values in the range of -21.8 to -15.7 and -19.2 to -16.3, respectively. The Girbhakar Formation which forms the top part of the Jodhpur Group has ε_{Nd} (0) in the range of -21.8 to -20.0. The carbonate sequences of the Bilara Group separate the Jodhpur Group from the overlying Nagaur Group. The ε_{Nd} (0) of the siliciclastic detritus separated from the Gotan Limestone of the Bilara Group vary in the range of -17.4 to -13.4. Sandstones at the lower part of the Nagaur Formation show ε_{Nd} (0) of -16.4 to -14.7, whereas that at the top of the Nagaur Formation has a value of -21.6. Sandstone samples from the Tunklian Formation, the topmost lithounit of the Marwar Supergroup, display a range of ε_{Nd} (0) values from -13.7 to -12.5, while the shale intercalated with the sandstone possesses a much lower value of -20.2. The Marwar sediments have lower radiogenic ε_{Nd} (0) values compared with that of the basement Malani rhyolites. The rhyolites and associated welded tuff of MIS display ε_{Nd} (0) of 0.2 and 6.7, respectively (Table 3.5). Samples from the potential sediment sources for the Marwar Basin show ε_{Nd} (0) in the range of -30.0 to -17.3 for the BGC-2, -16.1 to -10.4 for the

Erinpura Granites and -17.6 to -11.6 for the Delhi Supergroup. The Chhoti Khatu Tuff exhibits ε_{Nd} (0) from -21.1 to -20.3.

The $f^{Sm/Nd}$ of the Marwar sediments vary from -0.55 to -0.25; whereas that of the MIS rhyolite and Erinpura Granites varies from -0.33 to -0.29 and -0.40 to -0.12, respectively. Similarly, the $f^{Sm/Nd}$ of the BGC-2 and the Delhi Supergroup rocks varies in similar ranges: from -0.44 to -0.32 and -0.37 to -0.12, respectively (Table 3.5). The Depleted Mantle model ages (T_{DM}) of the Marwar sediments range from 1.2 to 2.8 Ga with a mode at 2.0 Ga. Among the basement rocks, the Malani Rhyolites have a narrow range of T_{DM} from 0.9 to 1.0 Ga and the Erinpura Granites show a wide range of T_{DM} from 1.6 to 2.1 Ga. The T_{DM} of BGC-2 varies from 2.6 to 2.9 Ga whereas the average T_{DM} of Chhoti Khatu Tuff is 2.3 Ga (Table 3.4).

3.6 Discussion

3.6.1 Age constraints on the Marwar sedimentation

The very presence of the Chhoti Khatu felsic tuff between the Sonia and Girbhakar formations suggests that the Marwar basin had remained volcanically active even after significant amount of sedimentation, well beyond the last phase of the basement volcanism. Based on detrital zircon geochronology, Xu and Meert (2014) had suggested a maximum age of ~702 Ma for the deposition of the tuff. This is consistent with the Rb-Sr whole rock isochron age of 703±40 Ma, determined by us. It was generally believed that the sedimentation in the Marwar basin got initiated in the Ediacaran period, ~115 Ma after the Malani magmatism. The lack of physical evidence for Neoproterozoic global glaciations in the Marwar basin was often cited as the rationale behind this argument (see Davis et al., 2014; Turner et al., 2014). However, the new age information suggests that the deposition of the Marwar Supergroup began very much during the Cryogenian period and that the perceived hiatus between the MIS and Marwars may not have been that long after all.

As discussed in the section 3.5.2, the lowest $^{87}Sr/^{86}Sr$ of 0.708097 displayed by the Gotan Limestone places its deposition time at ~570 Ma, in the late Ediacaran Period. The newly determined ages of the Chhoti Khatu Tuff and Gotan Limestone suggest that either there were protracted depositions of the Girbhakar and Dhanapa formations or there exists a depositional hiatus between the Jodhpur and Bilara groups. Since the Sonia and Girbhakar formations are largely fluvial sandstones a protracted deposition of the Girbhakar is unlikely and therefore, we believe that there may have been a cessation in deposition for about 100 Ma after the deposition of the Jodhpur Group.

3.6.2 Carbon isotopic variations in the Bilara Group

The variations in $\delta^{13}C$ with depth of the Gotan Limestone and the Pondlo Dolostone are shown in Fig. 3.10. The $\delta^{13}C$ transects of both Gotan and Pondlo formations are arranged in the order from proximal basin platform in the south to the distal basin slope northwards and are correlated based on the available geochemical and stratigraphic markers. Considering that some of the scatter in the data could be due to alteration, we used geochemical filters $\delta^{18}O$ >-10‰ and Mn/Sr <10 (Knoll et al., 1995) to discard secondary signals from interpretations.

We make the following observations from the temporal variations of $\delta^{13}C$ observed in various sections of the Bilara Group. 1) The $\delta^{13}C$ of the Gotan Limestone largely remained at 0‰ in the lower parts of the formation before it increased to ~2‰ in some of the sections while it remained at ~0‰ in others; and plunged into near mantle $\delta^{13}C$ value of ~-5‰ and recovered to the pre-excursion values (Fig. 3.10). 2) This $\delta^{13}C$ negative excursion is recorded throughout the basin and can be correlated between transects that are widely separated, from the proximal facies in the south to the distal facies towards the center of the basin (Fig. 3.10). This rules them out being the result of lateral facies variation. 3) The consistency of the $\delta^{13}C$ excursion throughout the basin suggest that it is the result of temporal change in the ocean chemistry and thus of global significance.

A number of such events were reported in the late Neoproterozoic (Halverson and Shields-Zhou, 2011; Narbonne et al., 2012; Xiao et al., 2016). Considering that the Gotan Limestone was deposited at ~570 Ma ($^{87}Sr/^{86}Sr$ = 0.7081) in the late Ediacaran, the $\delta^{13}C$ excursion is unrelated to the Cryogenian 'snowball Earth' events (i.e., the Marinoan glaciation). Also, unlike the Shuram anomaly, where the $\delta^{13}C$ drops to ~-12‰ (Grotzinger et al., 2011) and recovers slowly, the excursion here goes down only up to ~-5‰ and recovers back to 2‰. Bearing in mind the age constraints provided by the Sr isotope stratigraphy and the proximity of Indian shield to the Arabian-Nubian shield, Australia, and South China – locations from where

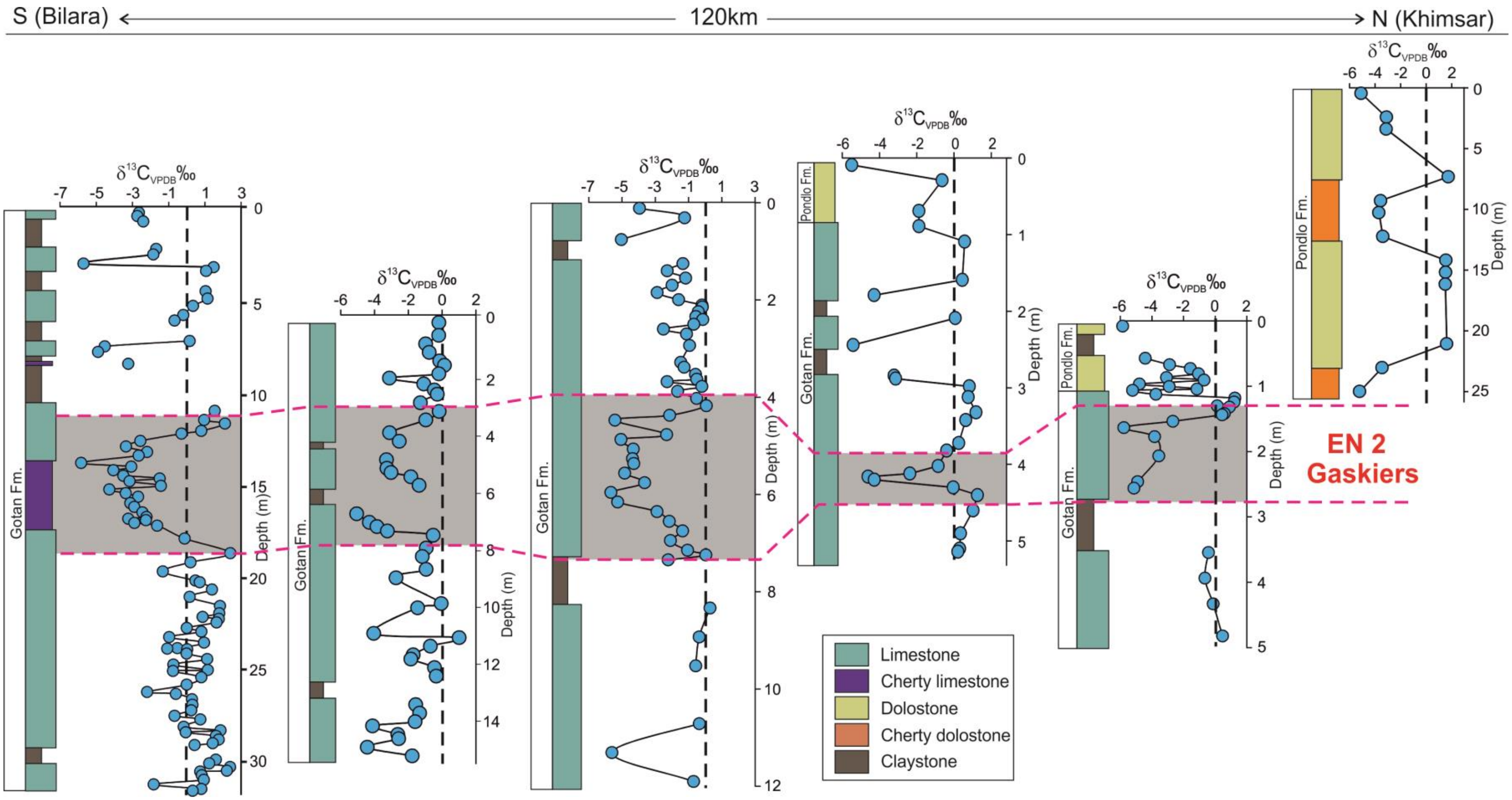

Figure 3.8: Variation of carbon isotopic composition ($\delta^{13}C$) with depth of the Gotan Limestone of the Bilara Group. The grey shaded region shows Ediacaran Negative excursion – 2 (EN2), the chemical signature of Gaskiers glaciation.

Ediacaran $\delta^{13}C$ excursions were reported, we suspect this could be the Ediacaran Negative excursion – 2 (EN2), the chemical signature of the ~580 Ma Gaskiers glaciation (Fig. 3.10; Narbonne et al., 2012; Xiao et al., 2016).

This has significant implications in our understanding of the oceanic conditions during the Gaskiers glaciation. Firstly, the Gotan Limestone lacked any physical signatures of a glaciation such as dropstones or diamictites, but, still preserved the chemical signal in the form of $\delta^{13}C$ excursion. Secondly, recent geochronological constraints suggest a shorter duration of <0.34 Ma for the Gaskiers glaciation (Pu et al., 2016). There were also doubts about the global nature of the glacial event with some suggesting it could be regional like the Phanerozoic glaciations (Pu et al., 2016). The paleomagnetic data from the Jodhpur and Nagaur groups have been interpreted to suggest an equatorial position for the Indian shield during Ediacaran (Davis et al., 2014), and therefore our result points to the scenario that the signals of glaciation were preserved even at the equatorial landmasses. This suggests that the Gaskiers glaciation was truly global in nature and the Ediacaran Ocean had faithfully recorded this extreme condition in the global climate despite its shorter duration and lesser aerial extent than the preceding glaciation (i.e., Marinoan).

3.6.3 Provenance of the Marwar sediments

The trace elemental patterns of siliciclastic sediments of the Marwar Supergroup are akin to average upper continental crust with typical enrichments in Th, U and Pb and depletions in Nb, Ta and Sr albeit the fact that their overall contents have been lowered as a result of dilution by presence of significant amount of quartz (Fig. 3.8). There is a significant enrichment in the LREE [La_N/Yb_N = 4.7 to 27.4] and a very high Th/Sc ratio (0.88 to 8.80); all indicative of predominance of felsic igneous rocks in the provenance (Figs. 3.8B and 3.11A). The Th/Sc vs Zr/Sc plot (Fig. 3.11A) shows a minor enrichment in the Zr concentration away from the compositional variation line, which suggests that there had been heavy mineral addition into the sediments due to recycling. These sediments also exhibit a large diversity in Sm/Nd ratio (represented as $f^{Sm/Nd}$) reflecting their derivation from less differentiated sources and poor mixing prior to deposition (McLennan and Hemming, 1992). In addition, there is a large variation in ε_{Nd}(650 Ma) (Fig. 3.12) and T_{DM} ages (Fig. 3.13) of the Marwar sediments which suggests that multiple sources of varying ages contributed detritus to the basin. Marwar sediments display a continental crustal character (Fig. 3.11A, B); however the overlapping nature of their Nd isotopic ratios with that of the Archean and Paleoproterozoic rocks in the vicinity suggests that these sediments were derived from local sources. The paleocurrent analyses (Awasthi and Parkash, 1981; Chauhan et al., 2004, 2001) in the Sonia and Girbhakar formations support such an inference by suggesting paleoflow directions from west-southwest, therefore implying that the sources were located along the eastern fringes of the basin.

The central and northwestern part of the basin is largely developed over the MIS, which includes bimodal volcanics dominated by rhyolite and minor exposures of granites. Since the MIS forms the basement in most parts of the basin, the rhyolites are expected to be the major contributor to the sediments. However, there exists a large disparity of T_{DM} distribution and Nd isotopic composition between the Marwars and the MIS [(ε_{Nd} (650 Ma) = -15.4 to -0.5, T_{DM} = 1.2 Ga to 2.8 Ga), (ε_{Nd} (650 Ma) = 3.4 to 6.2, T_{DM} =0.9 Ga to 1.5 Ga)] (Figs. 3.12, 3.13). All the younger T_{DM} ages (1.2 Ga to 1.7 Ga) and higher ε_{Nd} (650 Ma) values are reported from the samples collected at the contact between the Malani rhyolite and Sonia Formation suggest that the basement's influence, if any, was limited only to the sediments deposited immediately above it. The Erinpura Granites form the basement in the eastern parts of the Marwar basin. Their ε_{Nd} (650 Ma) and T_{DM} clearly overlap with that of the Marwars (Fig. 3.12, 3.13), which when considered along with the results of paleocurrent analysis (east to west) suggests that these granites have been a major source for the Marwar sediments. Rocks of the Delhi Supergroup also show overlapping ε_{Nd} and T_{DM} with that of the Marwars (Figs. 3.12, 3.13); however, together with the Erinpura Granites these sources cannot explain the entire observed ranges of the Marwar sediments. As suggested by ε_{Nd} (0) vs. Th/Sc and $f^{Sm/Nd}$ vs. ε_{Nd} (0) plots (Fig. 3.11), another major Paleoproterozoic source is required to explain the high T_{DM} values and ε_{Nd} (650 Ma) values in the Marwars. The BGC-2 fits into this description (Fig. 3.12) and its very presence at the eastern margin of the basin (Fig. 3.1) could have made it a major provenance for the Marwar sediments during the Neoproterozoic.

We have made an attempt to quantify the relative contributions of various sources to the Marwar Basin using ε_{Nd} and Gd/Yb. The latter is chosen since the middle and heavy REE's are known to be resistant to weathering and alteration. ε_{Nd} was corrected to time of deposition of the

Jodhpur, Bilara and Nagpur Groups and Gd/Yb were Chondrite normalized. Ternary mixing curves have been generated assuming the MIS, BGC-2 and Delhi Supergroup/Erinpura Granites as three end-member components in the ε_{Nd} (T) vs. Gd_N/Yb_N plots (Fig. 3.14). Three separate plots have been used for the three Groups of Marwar Supergroup (Fig. 3.14). From the three component mixing plots in Fig. 3.14, we make the following observations:

1. In spite of its close proximity, the MIS had very limited, if any, contribution to the sediment budget of the entire Marwars; except for at the depositional sites very near to the contact of the topmost MIS and bottommost Marwars (Sample 13, 17 in Fig. 3.14A),

2. Rocks of the Delhi Supergroup had remained a constant source of sediments (>30% of the total budget) to the Marwar Basin throughout its depositional history, including the time when fluvial activity was at its lowest, i.e. during the deposition of the Gotan Limestone Formation (Fig. 3.14B),

3. Contributions of the Erinpura Granites were probably limited to the Jodhpur Group, however, it is difficult to rule out complete absence of sediments derived from these, in the younger Groups,

4. The BGC-2 was one of the major sources of sediments to the Jodhpur Group (up to 70% of the total budget), however, its contribution to the basin appears to have ceased subsequent to the deposition of the Girbhakar Formation,

5. While the fluvial activity was virtually non-existent during the deposition of carbonates of the Bilara Group, some amount of siliciclastics did make it into the basin. The composition of these sediments (Fig. 3.14B) suggests that these were rich in heavy minerals (e.g., garnet) and were primarily derived from the Delhi Supergroup.

The variations of $^{87}Sr/^{86}Sr$ in the Marwar siliciclastics (Fig. 3.15) appear to suggest that very little recycling of sediments had happened from the Jodhpur Group into the Nagaur Group. Although it is difficult to compare the present day $^{87}Sr/^{86}Sr$ of the sediments with that of the potential sources, because of the differential weathering of minerals in the sources, it is quite clear that the sediments in the Jodhpur Group have a strong signal of being derived from the

Delhi Supergroup and the BGC-2 (Fig. 3.15). The $^{87}Sr/^{86}Sr$ of the Nagaur sediments appears to have a signal of mixed sources (Fig. 3.15).

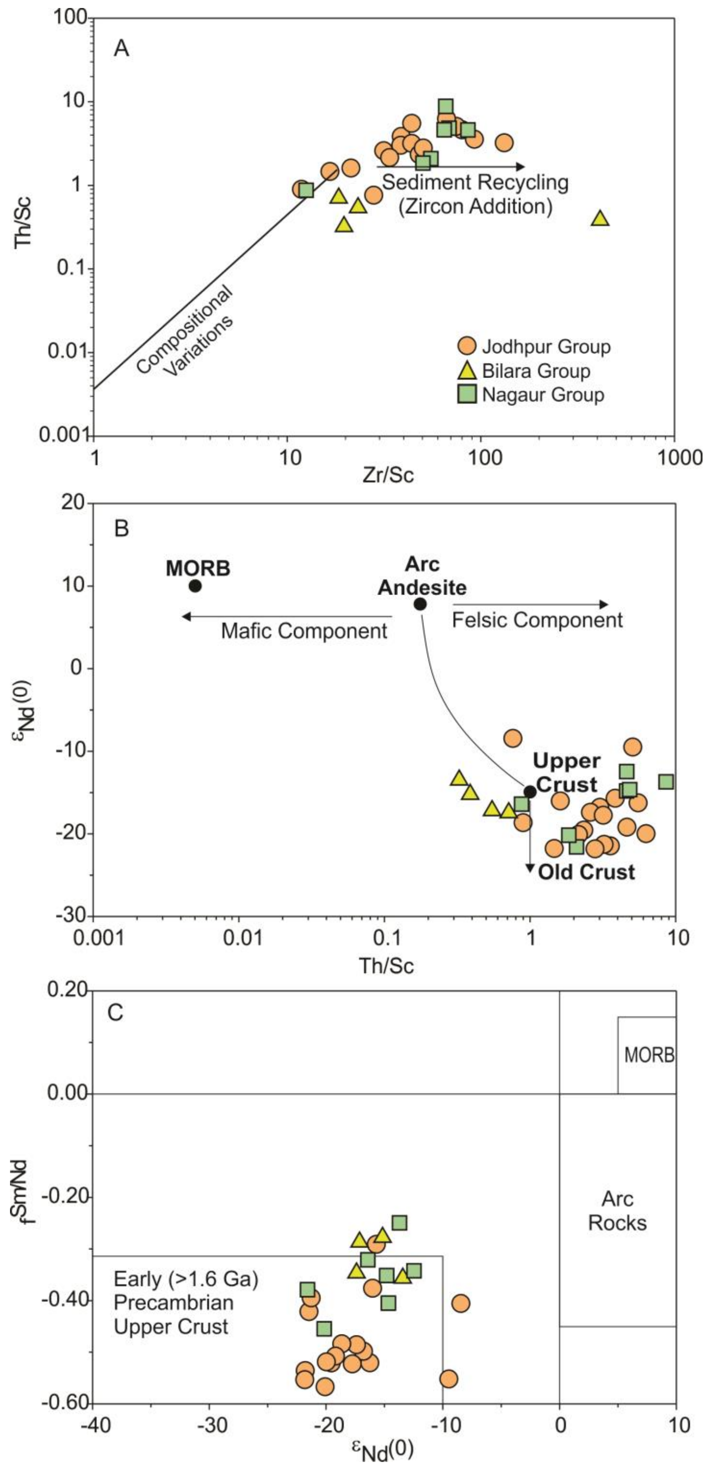

Figure 3. 9: Plots of Th/Sc vs. Zr/Sc (A), ε_{Nd} (0) vs. Th/Sc (B), and $f^{Sm/Nd}$ vs. ε_{Nd} (0) (C) for samples from siliciclastic formations of the Marwar Supergroup.

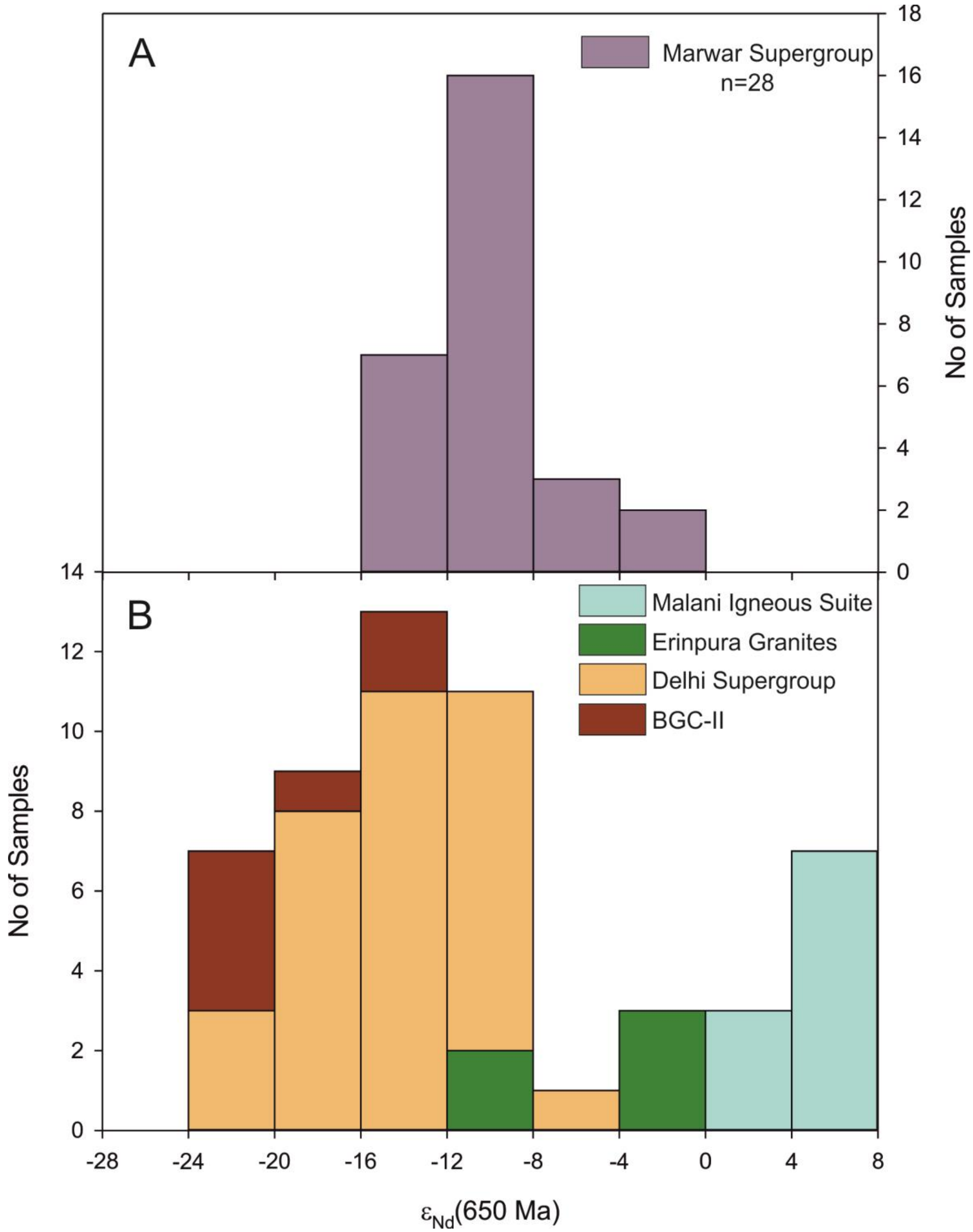

Figure 3.10: (A) Histogram of ε_{Nd} (t=650 Ma) distribution for the Marwar Supergroup (B) ε_{Nd} (t=650 Ma) distribution for the potential sources in a stacked histogram. MIS rhyolite, Erinpura Granites, Delhi Supergroup and BGC-2 data are from Carter, (2005); Kaur et al., (2007, 2009, 2011a); Tobisch et al., (1994); Van Lente et al., (2009) and this study (Table 3.5).

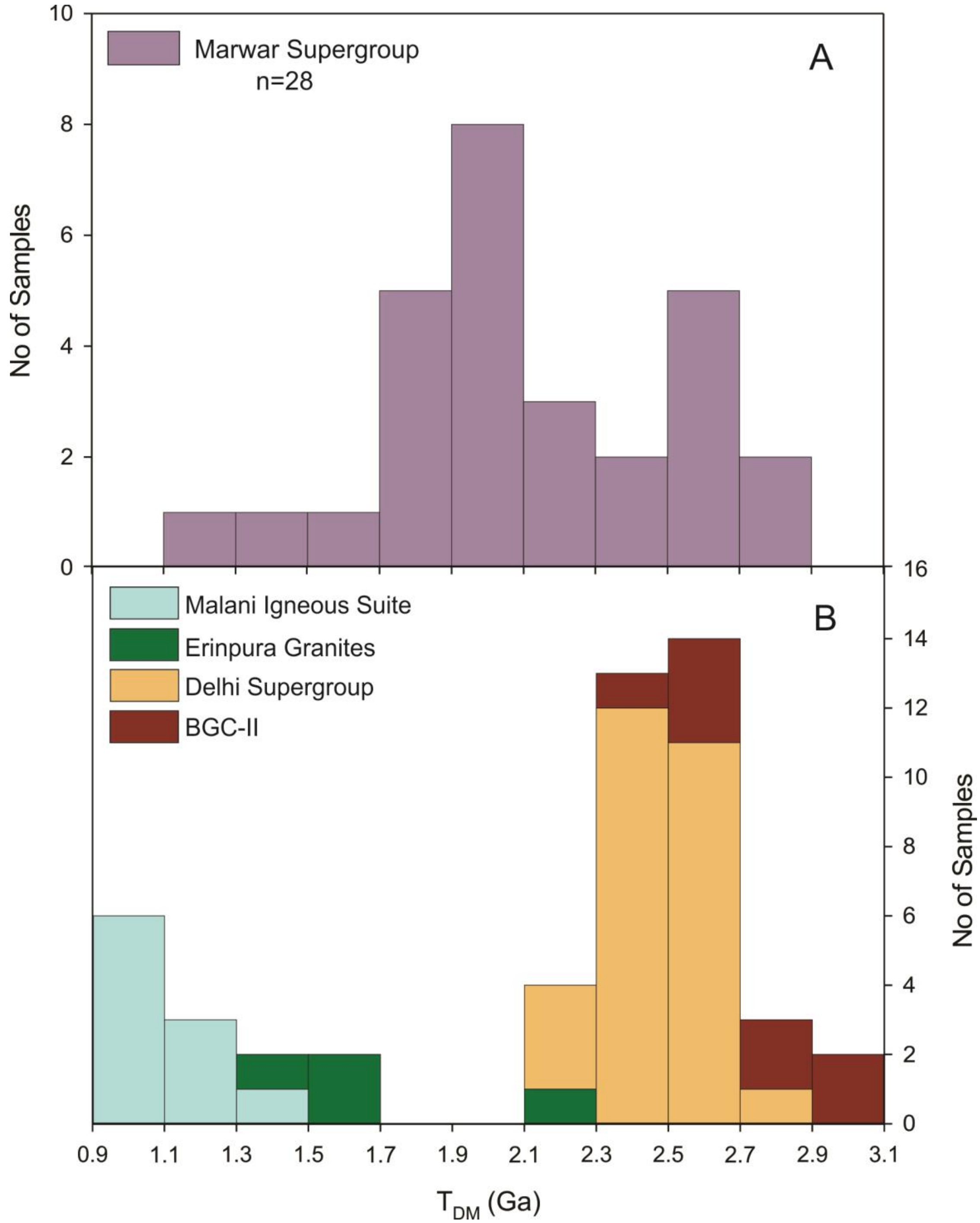

Figure 3.11: (A) Histogram of T_{DM} distribution for the Marwar Supergroup (B) Stacked histogram of T_{DM} distribution for the potential sources. Data sources as in Fig. 3.12.

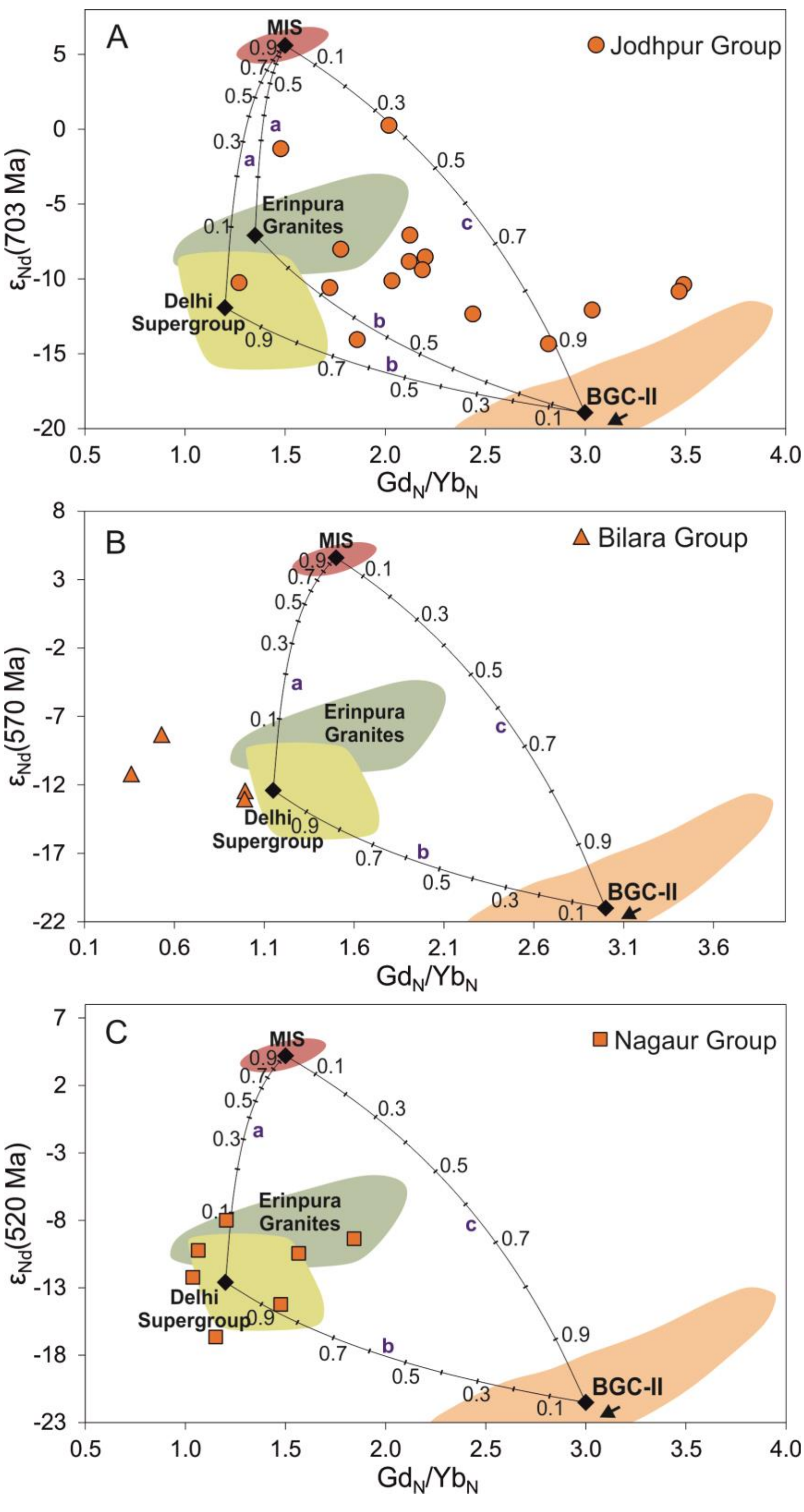

Figure 3.12: Plot of ε_{Nd} (T) vs. Gd_N/Yb_N for Marwar siliciclastics in the (A) Jodhpur Group, (B) Bilara Group, and (C) Nagaur Group. Mixing curves are generated with MIS, Delhi Supergroup/Erinpura Granites and BGC-2 as end members. Mixing curves a, b, and c, are drawn for Nd/Yb ratios of 0.25, 2, and 2, respectively, for all the three plots. Data sources: as in Fig. 3.12.

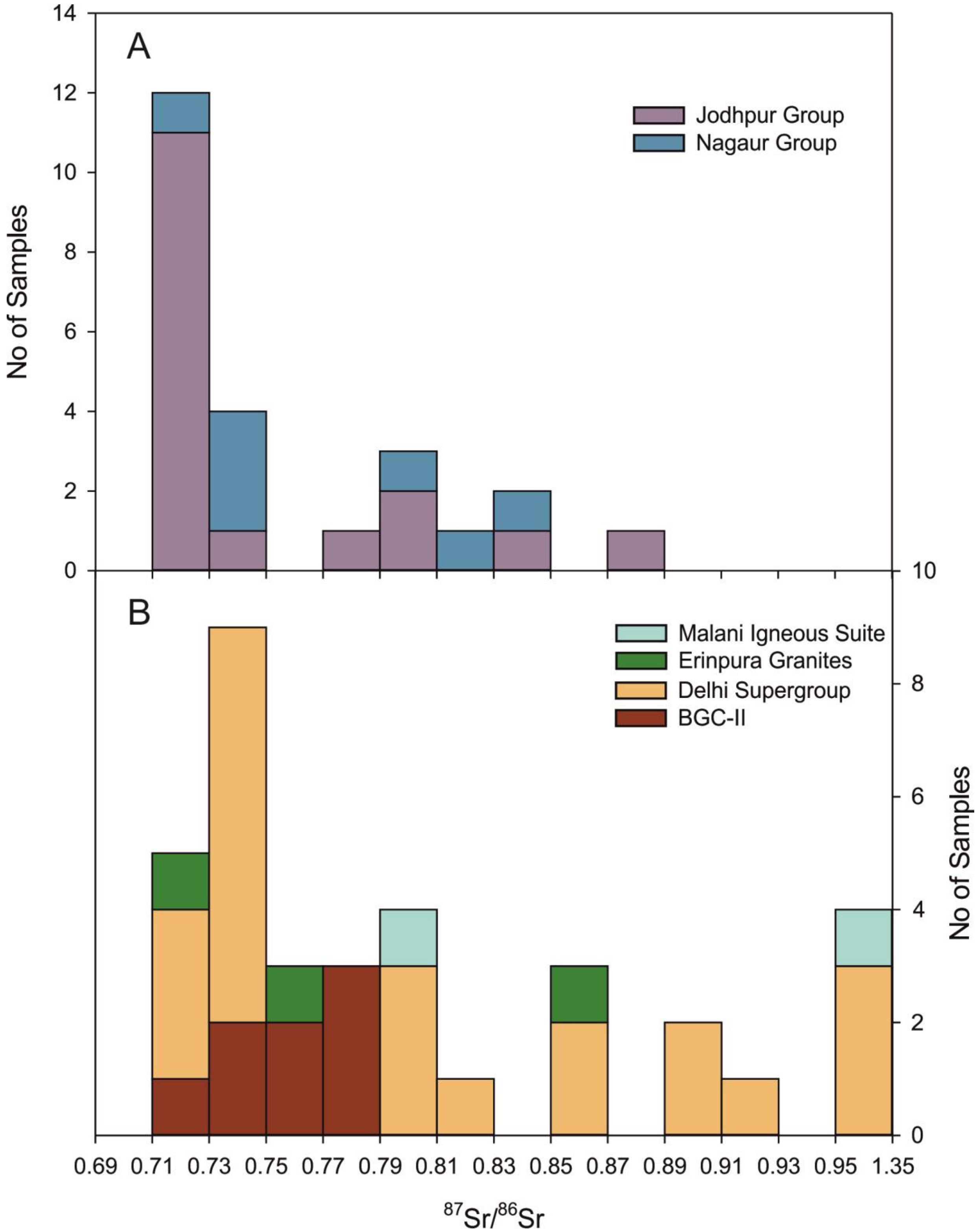

Figure 3.13: Stacked histogram of $^{87}Sr/^{86}Sr$ for the Jodhpur and Nagaur Groups (A) compared with $^{87}Sr/^{86}Sr$ of potential source regions (B). Data sources: as in Fig. 3.12.

3.6.4 Origin of the Chhoti Khatu Tuff

In the Primitive Mantle normalized diagram, the samples from the Chhoti Khatu Tuff show depletions in Sr, Eu, Nb, Ta, and enrichment in Pb indicating their crustal character (Fig. 3.9). Their dominantly felsic character is evident from the LREE enriched patterns in the Chondrite normalized plot, with La_N/Yb_N ratio ranging from 6.6 to 10.9 (Fig. 3.9). They display relatively flat HREE patterns with an average Gd_N/Yb_N = 1.2, and show conspicuous negative Eu anomalies with an average [Eu/Eu*] = 0.56 (Fig. 3.9). The $^{87}Sr/^{86}Sr$ and ε_{Nd} (0) of the tuff vary from 0.8993 to 0.9445 and from -21.1 to -20.3 respectively, and an average T_{DM} of 2.3 Ga (Table 3.4). The trace element and isotopic data indicate that the tuff is of upper continental crust origin and most likely to have been derived from the surrounding cratonic basement rocks.

As discussed in section 3.6.1, the age of deposition of the Chhoti Khatu Tuff is constrained to be 703±40 Ma (2σ). The reported ages for Malani magmatism vary from 771 – 681 Ma; however, the major phase of volcanism is considered to have occurred between 770 – 750 Ma (Gregory et al., 2009). Meert et al., (2013) reported a minimum age of ~704 Ma for the terminal dyke phase of the Malani magmatism, whereas a younger age of 681±20 Ma (2σ) was reported from the ultrapotassic rhyolites of Manihari (Rathore et al., 1999). They indicate that the pulses of volcanism related to the MIS could have extended for several millions of years. These younger Malani ages overlap with the age of deposition of the Chhoti Khatu Tuff even though the calcareous tuff is separated from the voluminous Malani volcanics by the Sonia Formation. In order to ascertain whether the Chhoti Khatu Tuff is an extension of the Malani magmatic activity, we compared the trace element patterns, and the Sr and Nd isotopic compositions of the Chhoti Khatu Tuff, corrected for its age of deposition, with that of the rhyolites and the welded tuffs of the Malani volcanics.

Although, the Chhoti Khatu Tuff possess similar trace element pattern as that of the Malani volcanics, they show a noticeable Pb enrichment, a lower Eu anomaly ([Eu/Eu*] = 0.56), and a much lower total REE concentration than that of the Malani volcanics. The isotopic composition of the tuff, when corrected for the age of deposition, shows an average $^{87}Sr/^{86}Sr$ (703 Ma) of 0.7587 and ε_{Nd} (703 Ma) of -13.0 (Fig. 3.16), whereas the Malani volcanics display $^{87}Sr/^{86}Sr$ (703 Ma) between a meaningless 0.6632 and 0.7350 and ε_{Nd} (703 Ma) between -4.3 and 6.6

(Carter, 2005; George and Ray, 2017). The Sr isotope system of the Malani volcanics is altered but it doesn't change the interpretations. Also, the Malani volcanics display T_{DM} of ~1.0 Ga ascertaining its Neoproterozoic origin, whereas the tuff samples show T_{DM} of ~2.3 Ga suggesting a much older Paleoproterozoic lineage. From the geochemical data, it is conspicuous that the Chhoti Khatu Tuff is not an extension of the proximal voluminous Malani volcanics, and had been derived most likely from an older Paleoproterozoic crust possibly similar to BGC-2 (Fig. 3.16).

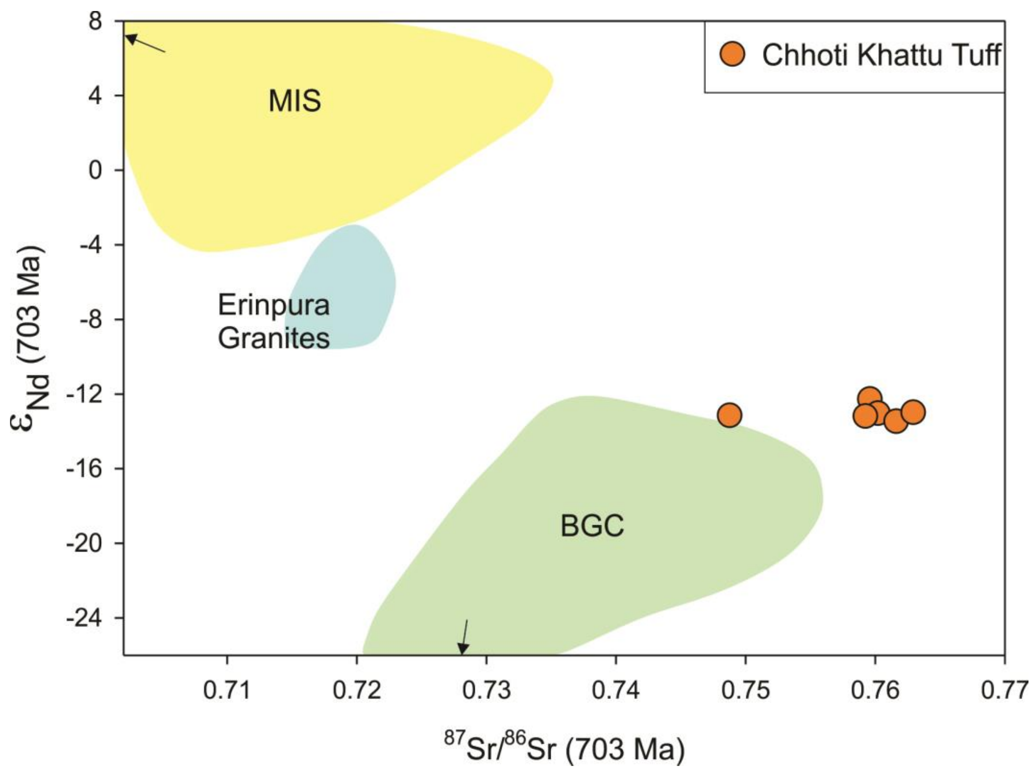

Figure 3.14: Plot of ε_{Nd} (t=703 Ma) vs. $^{87}Sr/^{86}Sr$ (t=703 Ma) of the Chhoti Khatu Tuff. Data sources: as in Fig. 3.12.

3.6.5 Evolution of the Marwar basin and global correlations

The Rb-Sr whole rock isochron age of 703±40 Ma obtained for the Chhoti Khatu tuff indicates that the sedimentation in the Marwar Basin began shortly after the Malani magmatism. The sedimentation started in the Cryogenian, and not in the Ediacaran Period, as believed earlier. The provenance study suggests that the Delhi Supergroup, BGC-2 and possibly the Erinpura Granites acted as the major sediment sources to the Jodhpur Group. Various trace element ratios and Nd isotopic composition capture the change in mineralogy of the provenance over the course of the sedimentation (Fig. 3.17). The $f^{Sm/Nd}$ decreases and Gd_N/Yb_N increases stratigraphically upward in the Jodhpur Group (Fig. 3.17), which suggest dominance of contributions from Early Precambrian crustal rocks, in this case the BGC-2. The decrease in ε_{Nd} (0) from bottom to top (from -9 to -21) within the formation supports the above inference. This information, results of paleocurrent analysis, and the predominantly fluvial nature of the sediments clearly suggest that the sediments in the Jodhpur Group were derived from the Aravalli Mountain Ranges which incorporated all the above mentioned lithologies, got deposited on the Erinpura Granites in the eastern fringes of the basin and covered the MIS in the central and western parts of the basin (Fig. 3.18). This also explains the lack of contribution of MIS to the Marwar sedimentation beyond a few beds at the basement-cover contact. It appears that the topography of the area had already attained almost the current configuration by the time the development of the basin had begun.

However, the basin remained volcanically active as suggested by the Chhoti Khatu felsic tuff, which marks the end of sedimentation in the Sonia Formation. The deposition of the tuff was followed by a change in facies from the marginal marine realms of the upper Sonia Formation to a more coarse and pebbly sandstone in form of the Girbhakar Formation, which is a braided fluvial deposit. The new age constraints given by us, the paleomagnetic data (Davis et al., 2014) and age distribution of detrital zircons (McKenzie et al., 2011; Turner et al., 2014) allow us to correlate the evolution of the Marwar basin with a host of terminal Neoproterozoic-Early Cambrian basins worldwide, developed along similar equatorial paleolatitudes (Fig. 3.19). The Jodhpur Group could have evolved contemporaneously with the Arkahawl Formation of the Huqf Supergroup, the Nagthat Formation (Juansar-Simla Groups) of Lesser Himalayas and the Wukiangxi Formation (Liantuo Formation-Banxi Group) of South China; all of which are dominated by both fluvial and shallow marine sandstones, and siltstones (Jiang et al., 2003; Rieu et al., 2007 and the references therein). There is no equivalent succession developed in the Salt Range of Pakistan (Gee, 1989; Krishnan, 1966). This marks the first phase in the evolution of the Marwar basin.

The second phase of the basin expansion started with the deepening of the basin and deposition of the Bilara carbonates at ~600 Ma (Fig 3.18B), after a hiatus of ~100 Ma. The break in sedimentation also explains the lack of any physical evidence for the 635 Ma old, Marinoan Glaciation in the basin. The Hanseran Evaporite Group, a homotaxial equivalent of the Bilara

Group (Das Gupta, 1996) is often correlated with contemporaneous evaporite deposits of the Ara Group in the Huqf Supergroup and Salt Range Formation (Saline Series) in the Salt Range (Fig. 3.19) owing to similarity in carbonate-evaporite cycles (Cozzi et al., 2012). In addition, Mazumdar and Strauss, (2006) suggested that both Bilara and Hanseran Evaporite groups could be coeval due to the similarity in their Sr and S isotopic ratios. The age of the Ara Group was constrained to be 544±3 Ma (Brasier et al., 2000), and therefore, this age can be considered as the upper bound of the age of the Bilara Group.

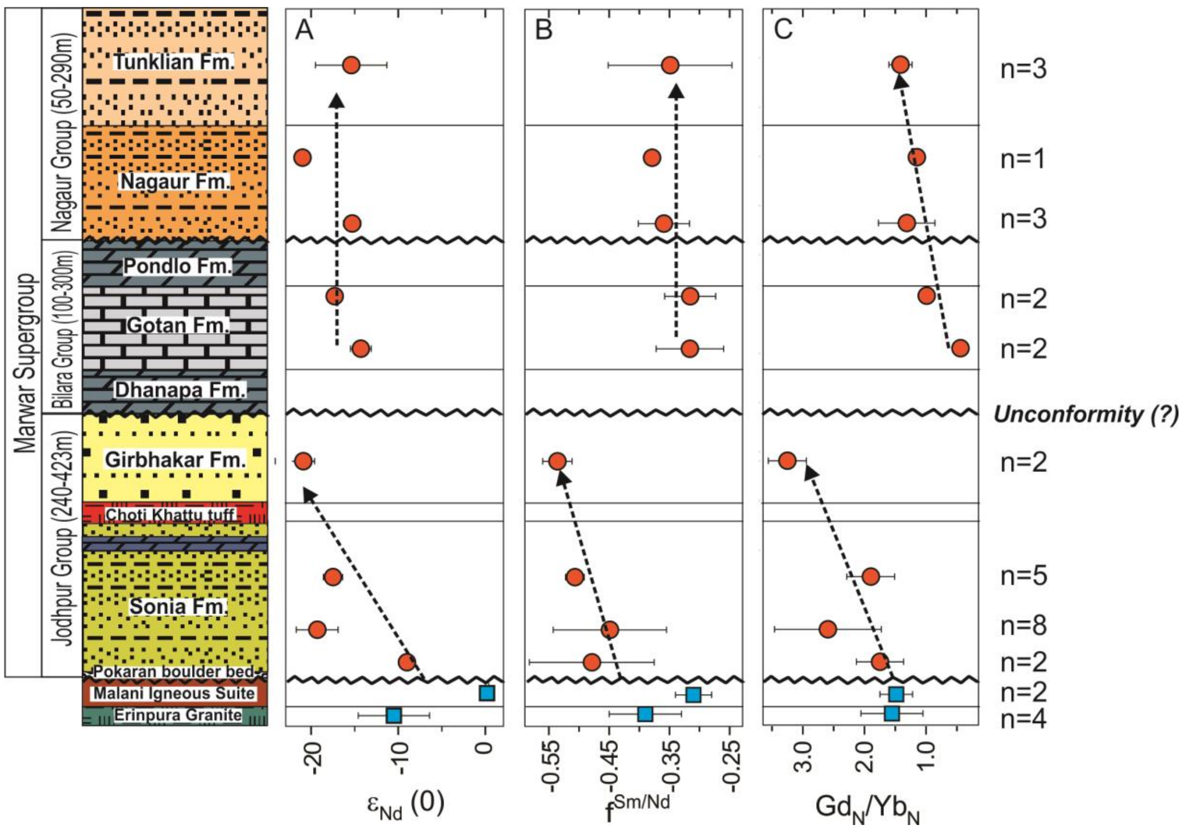

Figure 3.15: Variations of ε_{Nd} (0), $f^{Sm/Nd}$ and Gd_N/Yb_N with stratigraphy in the Marwar Supergroup. Error bars are 1σ.

This protracted carbonate sedimentation period ends with the resumption of clastic sedimentation with the deposition of fluvial sandstones of the Nagaur Group (Fig. 3.18C). The youngest detrital zircon age of ~540 Ma (McKenzie et al., 2011) and trace fossil assemblages (Kumar and Pandey, 2010) reported from the Nagaur Formation suggest that its deposition occurred mostly in the early Cambrian. These age constraints place the deposition of the Nagaur and Bilara Groups within the time frame of the Malagasy Orogeny when Indian shield collided

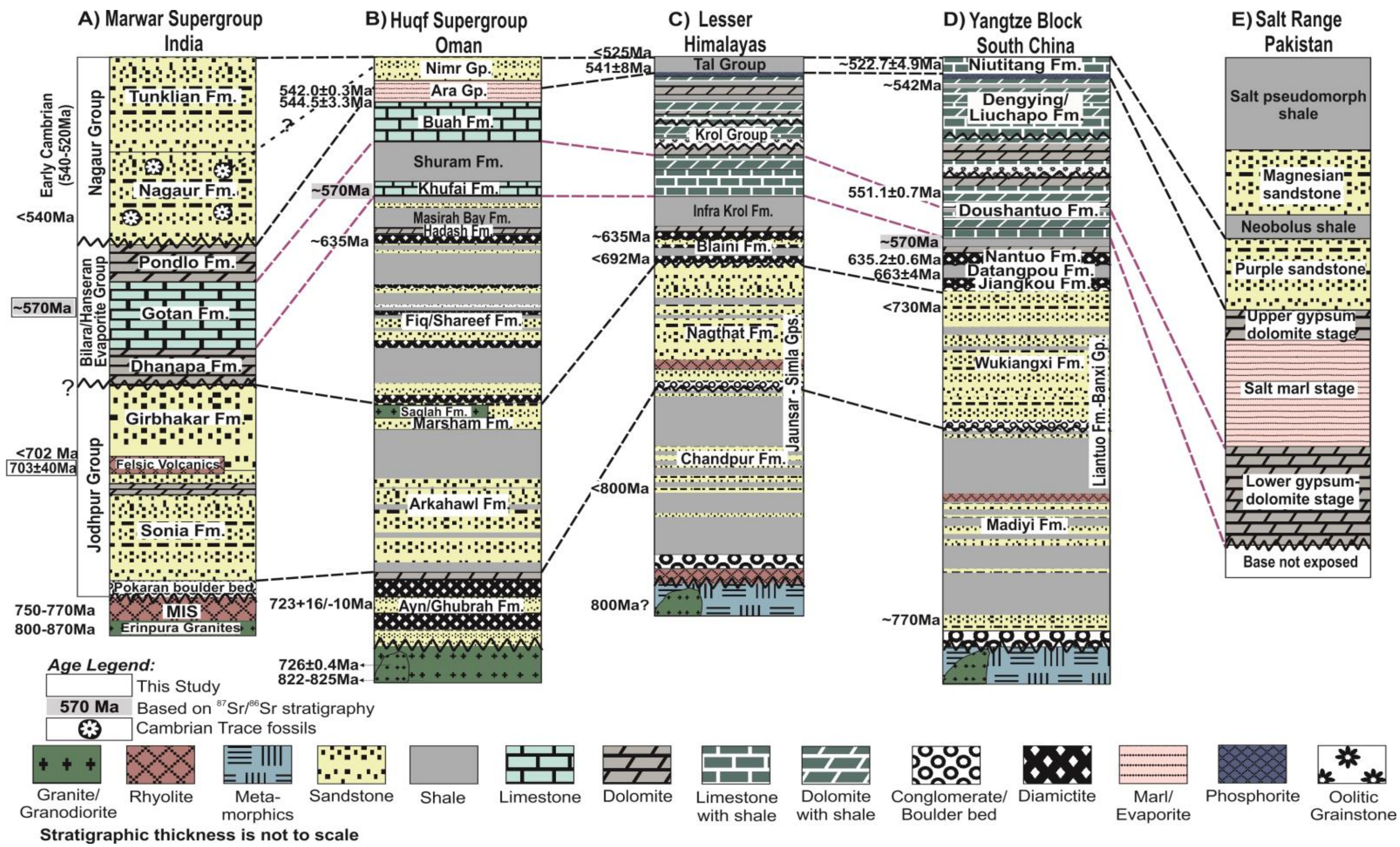

Figure 3.16: Comparative stratigraphy and proposed correlations between the Marwar Supergroup, the Huqf Supergroup of Oman, the Salt Range of Pakistan, the Lesser Himalayas and the Yangtze platform sequences of India and South China, respectively. The stratigraphic thicknesses are not to scale. Correlations are made mostly based on the available age data, similarity in detrital zircon distribution and paleogeography of the basins during the late Neoproterozoic-early Cambrian period. Stratigraphy, geochronological and paleomagnetic data: Marwar Supergroup – (Davis et al., 2014; McKenzie et al., 2011; Meert et al., 2013; Rathore et al., 1999) and present study]; Huqf Supergroup – (Kilner et al., 2005; Le Guerroue, 2006; Rieu et al., 2007 and the references therein); Lesser Himalaya – (Jiang et al., 2003; Klootwijk, 1979; McKenzie et al., 2011; Tripathy and Singh, 2011 and the references therein). Yangtze block, South China – (Jiang et al., 2011, 2007, 2003; Macouin et al., 2004; Wang et al., 2012 and the references therein). Salt Range – (Gee, 1989; Krishnan, 1966; McElhinny, 1970).

with the already amalgamated Azania and Congo–Tanzania–Bangweulu Block in the final stages of formation of Gondwana (Collins and Pisarevsky, 2005; Meert, 2003). The relapse of sedimentation in the basin is associated with a change not only in the depositional facies but also in the provenance. According to earlier studies, the Nagaur sandstones show less matured character owing to shorter transportation and hence derivation from proximal sources (Pareek, 1984 and the references therein). Our geochemical data also capture this change in provenance (Fig. 3.17). From a BGC-2 dominant provenance, sediments became more confined to the sources in the Delhi Supergroup and/or Erinpura Granites suggesting a major tectonic event in the region during 700 – 600 Ma. Since NW India remained stable during the East African Orogeny (Collins and Pisarevsky, 2005), it is quite likely this event could be linked to the initial stages of the Malagasy Orogeny, where peak metamorphic conditions existed during 510 – 550 Ma (Ashwal et al., 2013; Rathore et al., 1999; Sen et al., 2013). The new age constraint provided by Sr isotopic stratigraphy makes the Gotan Limestone contemporaneous with a host of late Ediacaran carbonate successions (Fig. 3.19), such as the Khufai-Shuram formations of Oman, the Lower Gypsum Dolomite stage of Salt Range, and lower part of the Krol Group and Doushantuo Formation of Lesser Himalayas and South China, respectively (Jiang et al., 2007; Le Guerroue, 2006; Tewari and Sial, 2007 and the references therein). Similarly, early Cambrian Nagaur Group can be correlated with the top part of the Ara Group and the overlying Nimr Group, the Tal Group, Purple Sandstone and the Shuijingtuo/Niutitang Formation of Oman, Lesser Himalayas, Salt Range and the Yangtze block of South China, respectively (Fig. 3.19).

3.7 Conclusions

From our geochemical study of the rocks from the Marwar Supergroup we conclude the following.

1. The age of formation of the Chhoti Khatu Tuff is 703±40 (2σ) Ma, which suggests that the sedimentation in the basin started in the Cryogenian.

2. Results of Sr isotope stratigraphy suggest a depositional age of 570 Ma for the Gotan Formation of the Bilara Group, which in turn points to a long depositional hiatus of ~100 Ma between the Jodhpur and the Bilara groups. The presence of this hiatus could be the reason for absence of any evidence for the Marinoan glaciation in the Marwar Basin.

3. The $\delta^{13}C$ stratigraphy of the Gotan Limestone shows a prominent basin-wide negative excursion, where $\delta^{13}C$ drops beyond -5‰. We believe that it represents the Ediacaran Negative excursion – 2 (EN2), a chemical evidence of the Gaskiers glaciation.

4. We propose a three phase evolution of the Marwar Basin: (1) formation of the basin subsequent to the disbanding of the Rodinia in the Cryogenian during which the deposition of Jodhpur Group took place, (2) deepening of the basin and carbonate deposition during and after the amalgamation of Gondwana in the late Ediacaran, following a depositional haitus of ~100 Ma, and (3) deposition of fluvial sand in a shallow marginal basin during the early Cambrian.

5. Geochemistry of siliciclastic sediments in the Jodhpur Group suggests that the detritus was primarily sourced from the Delhi Supergroup and the BGC-2, whereas the Bilara and Nagaur Groups formed from sediments from the Delhi Supergroup, with no sediment supply from the BGC-2. We find near absence of sediment supply from the Malani Igneous Suite, except at the immediate contact regions with the bottommost Marwars.

Table 3.1: Details of the samples from the Marwar Supergroup and adjacent basement rocks

Sample ID	Formation/Group	Location	Description
Marwar Supergroup			
MWR 14 1 1-7	Sonia Formation	N26.592; E73.423	Dolostone
MWR 14 2 1-9	Sonia Formation	N26.592; E73.423	Dolostone
MWR 12 1-10	Sonia Formation	N26.592; E73.423	Dolostone
MWR 14-1	Sonia Formation	N26.587; E73.414	Fine-grained sandstone
MWR 14-126	Sonia Formation	N26.382; E73.060	Shale
MWR 14-127	Sonia Formation	N26.382; E73.060	Fine-grained sandstone
MWR 14-129	Sonia Formation	N26.400; E73.052	Medium-grained sandstone (quartz-arenite)
MWR 14 131-133	Sonia Formation	N26.329; E73.002	Medium-grained sandstone (quartz-arenite)
MR 14-1	Sonia Formation	N26.553; E73.415	Shale
MR 14-2	Sonia Formation	N26.553; E73.415	Coarse-grained sandstone
MR 14-13	Sonia Formation	N26.938; E71.902	Shaly sandstone
MR 14-15	Sonia Formation	N26.319; E72.946	Medium-grained sandstone (quartz-arenite)
MR 14-17	Sonia Formation	N26.305; E73.019	Medium-grained sandstone (quartz-arenite)
MWR 15-1	Sonia Formation	N27.123; E74.304	Medium-grained sandstone (quartz-arenite)
MWR 15-2	Sonia Formation	N27.163; E74.353	Fine-grained sandstone
MWR 15-6	Sonia Formation	N27.163; E74.353	Shale
MWR 15 3-5,7-9	Chhoti Khatu Tuff	N27.163; E74.353	Calcareous rhyolitic tuff
MWR 14-128	Girbhakar Formation	N26.400; E73.052	Gritty sandstone
MR 14-5	Girbhakar Formation	N26.222; E73.688	Medium-grained sandstone
MR 14-7	Dhanapa Formation	N26.561; E73.745	Stromatolitic Dolostone
MWR 14 16-41	Gotan Formation	N26.667; E73.733	Limestone
MWR 14 47-95	Gotan Formation	N26.494; E73.800	Limestone
MWR 14 103-124	Gotan Formation	N26.881; E73.518	Limestone
MR 17 1-91A	Gotan Formation	N26.116; E73.740	Limestone
MR 17 92-141	Gotan Formation	N26.555; E73.772	Limestone
MWR 14 42-44	Pondlo Formation	N26.667; E73.733	Dolostone
MWR 14 96-102	Pondlo Formation	N26.881; E73.518	Dolostone
MWR 14 3 1-12	Pondlo Formation	N26.778; E73.650	Dolostone
MWR 14-13	Nagaur Formation	N26.785; E73.684	Gritty calcareous sandstone (arkose)
MWR 14 -14	Nagaur Formation	N26.785; E73.684	Coarse-grained sandstone (arkosic arenite)
MWR 14 -15	Nagaur Formation	N26.785; E73.684	Coarse-grained sandstone (arkosic arenite)
MR 14-11	Nagaur Formation	N28.402; E73.658	Fine-grained sandstone
MWR 14-45	Tunklian Formation	N26.637; E73.770	Shale
MWR 14-46	Tunklian Formation	N26.637; E73.770	Medium-grained sandstone (quartz-arenite)
MR 14-8	Tunklian Formation	N26.637; E73.770	Medium-grained sandstone (quartz-arenite)
Basement Rocks			
MWR 14-130	Malani Igneous Suite	N26.400; E73.052	Rhyolite
MR 14-14	Malani Igneous Suite	N26.594; E72.326	Rhyolite
MWR 14-134	Malani Igneous Suite	N26.303; E73.025	Welded Tuff
ERG	Erinpura Granite	N26.520; E73.387	Granite
Sirohi 14-1	Erinpura Granite	N24.874; E72.882	Granite gneiss
Sirohi 14-2	Erinpura Granite	N24.874; E72.882	Metagranite
PH 15-1	Delhi Supergroup	N25.554; E73.861	Calc silicate

Sample ID	Formation/Group	Location	Description
PH 15-2	Delhi Supergroup	N25.554; E73.861	Quartzite
PH 15-45	Delhi Supergroup	N25.073; E73.866	Quartzite
PH 15-28	Delhi Supergroup	N25.759; E74.061	Micaceous quartzite
PH 15-16	Delhi Supergroup	N25.624; E73.826	Schist
PH 15-30	Delhi Supergroup	N25.775; E74.042	Metapelite
PH 15-34	Banded Gneissic Complex-2	N26.089; E74.449	Biotite granite gneiss
PH 15-36	Banded Gneissic Complex-2	N26.093; E74.494	Granite gneiss
PH 15-37	Banded Gneissic Complex-2	N26.093; E74.597	Granite gneiss
PH 15-38	Banded Gneissic Complex-2	N26.098; E74.624	Granite gneiss

Note: Locations are given in degree.

Table 3.2: Rb-Sr whole rock data for the Chhoti Khatu Tuff

Sample	Rb(ppm)	Sr(ppm)	$^{87}Rb/^{86}Sr$	$^{87}Sr/^{86}Sr$
MWR 15-3	90.06	18.39	14.44	0.904225
MWR 15-4	84.27	17.89	13.88	0.899269
MWR 15-5	78.68	12.83	18.14	0.941002
MWR 15-7	65.31	10.59	18.25	0.944467
MWR 15-8	56.77	11.41	14.68	0.909963

Note: Rb and Sr concentrations were measured using Q-ICPMS. External reproducibility for Rb and Sr measurements were < 3% at 2σ level.

Table 3.3: Geochemical data of carbonate formations of the Marwar Supergroup

Sample ID	$\delta^{13}C_{VPDB}$(‰)	$\delta^{18}O_{VPDB}$ (‰)	Depth (m)	Mg/Ca	Ca/Sr	Mn/Sr	$^{87}Sr/^{86}Sr$
Sonia Formation			Top				
MWR 14-1-1	1.4	-0.5	0.05				
MWR 14-1-2	1.1	-1.0	0.10				
MWR 14-1-3	0.9	-1.3	0.14				
MWR 14-1-4	1.1	-1.6	0.19				
MWR 14-1-5	0.0	-3.1	0.24	0.39	5403	126	0.718671
MWR 14-1-6	-1.2	-4.9	0.29				
MWR 14-1-7	-1.3	-4.9	0.34				
			Top				
MWR 14-2-1	1.9	-0.7	0.02	1.21	4546	104	0.716933
MWR 14-2-2	2.1	-0.1	0.09				
MWR 14-2-3	2.3	0.3	0.12				
MWR 14-2-4	2.1	0.0	0.14				
MWR 14-2-5	2.1	0.0	0.16				
MWR 14-2-6	2.2	-0.2	0.18	0.39	3509	59	0.719939
MWR 14-2-8	2.4	0.6	0.25				
MWR 14-2-9	2.0	-0.8	0.39				
			Top				

Sample ID	$\delta^{13}C_{VPDB}$(‰)	$\delta^{18}O_{VPDB}$ (‰)	Depth (m)	Mg/Ca	Ca/Sr	Mn/Sr	$^{87}Sr/^{86}Sr$
MR 12-1	-1.2	-5.3	0.00				
MR 12-3	-4.7	-9.7	0.10				
MR 12-4	2.2	-0.5	0.25				
MR 12-5	2.4	0.0	0.32				
MR 12-6	1.1	-2.5	0.45				
MR 12-7	1.4	-2.2	0.50				
MR 12-8	1.1	-2.6	0.53				
MR 12-9	2.1	-0.3	0.63				
Dhanapa Formation							
MR 14-7	-1.9	-2.1		1.2	2375	1.2	0.709195
Gotan Formation			Top				
MR 17-1	-2.6	0.8	0.00				
MR 17-2	-2.7	1.9	0.18				
MR 17-3	-2.4	2.0	0.48				
MR 17-4	-1.7	0.5	1.98				
MR 17-5	-1.8	-0.7	2.28				
MR 17-6	-5.7	-6.6	2.78				
MR 17-7	1.5	0.7	2.98				
MR 17-8	1.1	2.1	3.18				
MR 17-9	1.0	3.9	4.18				
MR 17-10	1.1	3.7	4.58				
MR 17-11	0.4	7.4	4.98				
MR 17-12	-0.2	4.9	5.48				
MR 17-13	-0.7	4.5	5.78				
MR 17-14	0.2	0.8	6.78				
MR 17-15	-4.5	-1.7	7.08				
MR 17-16	-4.9	-1.2	7.38				
MR 17-17	-3.2	-1.8	7.73				
MR 17-18	1.5	0.4	10.73				
MR 17-19	1.0	0.2	11.23				
MR 17-20	2.1	6.3	11.43				
MR 17-21	0.8	4.9	11.83				
MR 17-22	-0.3	2.4	11.98				
MR 17-23	-2.6	-2.0	12.38				
MR 17-24A	-3.4	-3.4	12.68				
MR 17-24	-2.2	-1.7	12.98				
MR 17-25	-2.6	-0.8	13.18				
MR 17-26	-5.8	-2.9	13.58				
MR 17-27	-3.1	-0.8	13.78				
MR 17-28	-4.0	-4.9	13.98				
MR 17-30	-3.5	1.6	14.28				
MR 17-31	-1.5	2.3	14.43				
MR 17-32	-3.2	0.3	14.58				
MR 17-33	-1.4	-0.9	14.83				
MR 17-34	-4.3	-2.5	15.03				

Sample ID	$\delta^{13}C_{VPDB}$(‰)	$\delta^{18}O_{VPDB}$ (‰)	Depth (m)	Mg/Ca	Ca/Sr	Mn/Sr	$^{87}Sr/^{86}Sr$
MR 17-35	-3.4	0.1	15.23				
MR 17-36	-2.7	0.6	15.43				
MR 17-38	-3.1	-3.7	15.78				
MR 17-39	-2.9	-1.5	15.98				
MR 17-40	-2.4	-4.4	16.28				
MR 17-41	-2.2	-3.1	16.53				
MR 17-42	-3.2	-7.8	16.63				
MR 17-43	-2.3	-7.0	16.71				
MR 17-44	-2.9	-6.8	16.86				
MR 17-45	-1.6	-5.0	17.01				
MR 17-46	-0.1	-6.3	17.71				
MR 17-47	2.4	-4.6	18.51				
MR 17-48	0.2	-5.5	19.01				
MR 17-49	-1.3	-5.8	19.51				
MR 17-50	0.5	-5.3	20.01				
MR 17-51	0.7	-4.4	20.10				
MR 17-52	1.4	-7.1	20.50				
MR 17-53	0.2	-4.8	20.90				
MR 17-54	1.8	-4.6	21.40				
MR 17-55	1.8	-4.2	21.80				
MR 17-56	0.9	-5.6	22.00				
MR 17-57	1.8	-5.1	22.10				
MR 17-58	1.6	-3.1	22.30				
MR 17-59	0.0	-6.2	22.60				
MR 17-60	0.8	-7.1	22.80				
MR 17-61	-1.0	-2.9	23.10				
MR 17-62	1.0	-5.7	23.40				
MR 17-63	-0.5	-5.8	23.70				
MR 17-63A	-1.1	-6.2	23.73				
MR 17-63B	0.0	-5.2	23.76				
MR 17-64	0.0	-4.2	24.00				
MR 17-65	1.1	-4.3	24.30				
MR 17-66	-0.7	-4.1	24.60				
MR 17-67	1.2	-4.0	24.90				
MR 17-67A	-0.8	-4.8	24.95				
MR 17-68	0.8	-2.7	25.30				
MR 17-69	0.0	-4.3	25.70				
MR 17-70	-2.2	-6.3	26.10				
MR 17-71	-0.6	-4.6	26.20				
MR 17-72	0.3	-4.4	26.50				
MR 17-73	0.3	-3.8	26.80				
MR 17-74	0.3	-5.5	27.10				
MR 17-75	-0.7	-4.6	27.40				
MR 17-76	0.8	-4.6	27.60				
MR 17-77	-0.2	-1.1	28.00				

Sample ID	$\delta^{13}C_{VPDB}$(‰)	$\delta^{18}O_{VPDB}$ (‰)	Depth (m)	Mg/Ca	Ca/Sr	Mn/Sr	$^{87}Sr/^{86}Sr$
MR 17-78	1.9	0.3	28.20				
MR 17-79	-0.1	-5.4	28.30				
MR 17-80	1.6	-3.6	28.50				
MR 17-81	1.8	-3.6	28.70				
MR 17-82	1.4	-4.8	28.90				
MR 17-83	0.4	-6.1	29.00				
MR 17-84	1.6	-3.7	29.80				
MR 17-85	1.2	-3.7	30.00				
MR 17-86	2.4	0.9	30.20				
MR 17-87	2.2	-1.0	30.40				
MR 17-87A	0.7	-1.4	30.45				
MR 17-88	0.8	-1.3	30.65				
MR 17-89	0.9	-0.8	30.90				
MR 17-90	-1.8	-3.8	31.15				
MR 17-91	0.8	-3.2	31.40				
MR 17-91A	0.3	-6.4	31.50				
			Top				
MWR 14-47	-0.2	-0.4	0.00	0.90	689	0.04	0.711096
MWR 14-48	-0.2	2.3	0.45				
MWR 14-49	-1.0	1.0	0.75				
MWR 14-50	-0.8	3.1	1.05	0.35	797	0.1	0.710537
MWR 14-51	-0.1	-2.1	1.35				
MWR 14-52	0.2	2.1	1.50				
MWR 14-53	-0.2	1.6	1.80				
MWR 14-54	-3.1	-1.4	1.95	0.18	3891	0.4	0.709539
MWR 14-55	-1.1	-7.2	2.16	0.09	3497	0.5	
MWR 14-56	-0.5	-2.9	2.37				
MWR 14-57	-0.3	-3.4	2.52				
MWR 14-58	-1.3	-3.7	2.82				
MWR 14-60	-0.2	-3.9	3.12				
MWR 14-61	-1.0	-1.3	3.42				
MWR 14-62	-3.1	-10.8	3.87	0.02	3916	0.9	
MWR 14-63	-2.5	-11.4	4.17	0.01	5573	1.4	
MWR 14-64	-3.3	-3.9	4.82	0.03	1490	0.1	
MWR 14-65	-3.3	-4.6	5.12	0.01	1025	0.1	
MWR 14-66	-3.0	-4.8	5.27	0.02	1130	0.1	0.708143
MWR 14-67	-1.8	-2.9	5.42				
MWR 14-68	-1.4	-0.6	5.72				
MWR 14-70	-5.1	-8.8	6.72	0.003	4947	1.5	
MWR 14-71	-4.3	-5.6	7.02	0.002	5316	0.8	
MWR 14-72	-3.9	-5.0	7.17	0.003	4332	0.5	
MWR 14-73	-3.2	-4.7	7.32	0.003	2507	0.4	
MWR 14-74	-0.5	-1.8	7.47				
MWR 14-75	-0.9	-2.7	7.92				
MWR 14-76	-1.2	-1.8	8.22				

Sample ID	$\delta^{13}C_{VPDB}$(‰)	$\delta^{18}O_{VPDB}$ (‰)	Depth (m)	Mg/Ca	Ca/Sr	Mn/Sr	$^{87}Sr/^{86}Sr$
MWR 14-77	-0.9	-1.0	8.67				
MWR 14-78	-2.7	-2.5	8.97				
MWR 14-79	0.0	-0.6	9.87	0.02	2264	0.4	0.708111
MWR 14-80	-1.4	-4.4	10.02				
MWR 14-81	-4.0	-4.0	10.92	0.004	3344	0.7	
MWR 14-82	1.0	2.1	11.07				
MWR 14-83	-0.7	-3.7	11.37				
MWR 14-84	-1.7	-4.8	11.67				
MWR 14-85	-1.8	-5.4	11.82	0.005	3450	0.1	0.708525
MWR 14-86	-0.4	-4.2	12.12				
MWR 14-87	-0.3	-0.3	12.42	0.12	2937	0.2	0.708436
MWR 14-88	-1.6	-4.3	13.42	0.004	4083	0.3	
MWR 14-89	-1.3	-4.1	13.72				
MWR 14-90	-1.6	-4.4	14.02				
MWR 14-91	-4.1	-6.1	14.17	0.002	2586	0.1	
MWR 14-92	-2.6	-5.7	14.47	0.003	2854	0.1	
MWR 14-93	-2.6	-5.9	14.62				
MWR 14-94	-4.4	-7.4	14.92	0.003	3726	0.3	
MWR 14-95	-1.8	-5.1	15.22	0.01	2775	0.1	0.708367
			Top				
MR 17-92	-3.9	-9.4	0.00				
MR 17-93	-1.2	-1.7	0.20				
MR 17-94	-5.0	-6.8	0.65				
MR 17-95	-1.3	-2.4	1.15				
MR 17-96	-2.3	-3.3	1.30				
MR 17-97	-1.2	-1.5	1.45				
MR 17-98	-2.0	-4.3	1.60				
MR 17-99	-2.9	-4.0	1.75				
MR 17-100	-1.6	-3.5	1.90				
MR 17-101	-0.2	1.9	2.01				
MR 17-102	-0.2	1.0	2.05				
MR 17-103	-0.4	-0.3	2.15				
MR 17-104	-0.6	0.2	2.25				
MR 17-104A	-0.1	0.6	2.31				
MR 17-105	-0.7	-0.5	2.41				
MR 17-106	-2.5	-3.7	2.51				
MR 17-107	-1.1	-1.0	2.61				
MR 17-109	-0.9	-0.4	2.85				
MR 17-110	-1.5	-1.8	3.20				
MR 17-111	-1.3	-1.4	3.30				
MR 17-112	-0.6	-0.1	3.45				
MR 17-113	-0.5	0.1	3.55				
MR 17-114	-2.3	-2.1	3.60				
MR 17-115	-0.2	-1.2	3.70				
MR 17-116	-1.7	-2.7	3.80				

Sample ID	$\delta^{13}C_{VPDB}$(‰)	$\delta^{18}O_{VPDB}$ (‰)	Depth (m)	Mg/Ca	Ca/Sr	Mn/Sr	$^{87}Sr/^{86}Sr$
MR 17-117	-0.5	-1.7	3.95				
MR 17-118	0.1	-3.8	4.10				
MR 17-119	-2.1	-3.6	4.30				
MR 17-120	-5.4	-5.4	4.40				
MR 17-121	-2.3	-3.3	4.70				
MR 17-122	-5.1	-3.7	4.80				
MR 17-123	-4.3	-4.8	5.00				
MR 17-124	-4.4	-5.9	5.20				
MR 17-124A	-4.3	-6.0	5.30				
MR 17-125	-4.8	-4.9	5.50				
MR 17-126	-3.6	-5.8	5.70				
MR 17-127	-5.7	-5.9	5.90				
MR 17-128	-5.3	-5.8	6.10				
MR 17-129	-2.9	-3.2	6.30				
MR 17-130	-2.2	-3.7	6.50				
MR 17-131	-1.4	-1.5	6.70				
MR 17-132	-2.1	-3.1	6.90				
MR 17-133	-1.1	-2.4	7.10				
MR 17-133A	0.0	3.3	7.20				
MR 17-134	-2.2	-3.1	7.30				
MR 17-135	0.3	3.0	8.30				
MR 17-136	-0.4	0.9	8.90				
MR 17-137	-0.6	0.6	9.50				
MR 17-139	-0.4	-2.7	10.70				
MR 17-140	-5.6	-7.5	11.30				
MR 17-141	-0.7	2.6	11.90				
			Top				
MWR 14-41	-1.9	-3.1	0.80				
MWR 14-40	0.6	0.0	1.00	0.02	1551	0.03	0.708388
MWR 14-39	0.4	-2.4	1.50				
MWR 14-38	-4.3	-10.5	1.70	0.02	3678	0.6	
MWR 14-37	0.1	-0.1	2.00	0.02	1738	0.1	0.708097
MWR 14-36	-5.4	-9.6	2.35	0.01	7986	2.2	
MWR 14-35	-3.2	-5.0	2.75	0.004	3196	0.6	
MWR 14-34	-3.1	-6.6	2.79	0.004	3891	0.8	
MWR 14-33	0.8	0.0	2.89				
MWR 14-31	0.8	-2.1	3.03	0.03	1072	0.01	0.708153
MWR 14-30	1.2	-3.0	3.23				
MWR 14-29	0.6	-1.3	3.33				
MWR 14-27	0.3	-2.0	3.63				
MWR 14-26	-0.4	-3.0	3.73				
MWR 14-25	-0.9	-3.3	3.93				
MWR 14-24	-2.4	-5.1	4.03	0.01	3052	0.2	0.708190
MWR 14-23	-4.6	-11.3	4.07	0.01	6955	1.2	
MWR 14-22	-4.3	-5.6	4.11	0.01	2454	1.2	

Sample ID	$\delta^{13}C_{VPDB}$(‰)	$\delta^{18}O_{VPDB}$ (‰)	Depth (m)	Mg/Ca	Ca/Sr	Mn/Sr	$^{87}Sr/^{86}Sr$
MWR 14-21	0.0	-0.7	4.21				
MWR 14-20	1.3	-2.3	4.31				
MWR 14-19	1.0	-5.2	4.51				
MWR 14-18	0.4	-7.2	4.81				
MWR 14-17	0.3	-3.2	5.01	0.04	2609	0.1	0.708150
MWR 14-16	0.2	-3.9	5.05				
			Top				
MWR 14-103	-3.1	-5.7	0.80	0.003	3447	0.4	0.708290
MWR 14-103A	-0.7	-5.2	0.84				
MWR 14-104	-4.8	-10.1	0.90	0.005	8601	0.4	
MWR 14-105	-2.9	-10.1	0.94				
MWR 14-106	-1.1	-5.6	0.98				
MWR 14-107	-5.2	-9.8	1.00	0.004	9132	1.3	
MWR 14-108	-3.7	-5.5	1.06	0.01	3159	0.9	
MWR 14-109	1.2	-3.8	1.12	0.02	1069	0.03	0.708099
MWR 14-110	1.2	-4.1	1.18				
MWR 14-111	0.1	-4.5	1.24				
MWR 14-112	0.9	-2.7	1.26	0.02	1096	0.1	0.708099
MWR 14-113	0.6	-4.6	1.36				
MWR 14-114	0.4	-4.2	1.38				
MWR 14-115	-2.7	-6.9	1.48				
MWR 14-116	-5.8	-8.1	1.58	0.003	7580	1.1	
MWR 14-117	-3.8	-8.4	1.72	0.01	5872	0.5	
MWR 14-118	-3.6	-7.0	2.02	0.003	3895	5.3	
MWR 14-119	-4.9	-9.3	2.42	0.004	5718	1.2	
MWR 14-120	-5.1	-10.4	2.52	0.01	8032	0.8	
MWR 14-121	-0.4	-5.2	3.52	0.01	2790	0.2	0.708306
MWR 14-122	-0.6	-5.4	3.92				
MWR 14-123	-0.1	-4.6	4.32				
MWR 14-124	0.5	-6.4	4.82				
Pondlo Formation			Top				
MWR 14-44	-5.5	-4.3	0.00	0.12	9689	1.5	0.709530
MWR 14-43	-0.6	-1.9	0.20	0.70	3355	1.3	0.710223
MWR 14-42	-1.9	-2.7	0.60	0.18	4475	7.3	
			Top				
MWR 14-96	-5.8	-10.3	0.00	0.01	12397.959	4.3	
MWR 14-98	-4.4	-9.4	0.50	0.003	6983	0.4	0.708781
MWR 14-99	-2.9	-10.2	0.60	0.01	7636	0.8	
MWR 14-100	-1.6	-8.6	0.66				
MWR 14-102	-1.1	-6.6	0.74				
			Top				
MWR 14-3-1	-5.1	-8.8	0				
MWR 14-3-2	-3.1	-9.9	2				
MWR 14-3-3	-3.1	-7.1	3				
MWR 14-3-4	1.7	-1.3	7				

Sample ID	$\delta^{13}C_{VPDB}$(‰)	$\delta^{18}O_{VPDB}$ (‰)	Depth (m)	Mg/Ca	Ca/Sr	Mn/Sr	$^{87}Sr/^{86}Sr$
MWR 14-3-5	-3.6	-9.6	9				
MWR 14-3-6	-3.7	-9.6	10				
MWR 14-3-7	-3.4	-9.8	12				
MWR 14-3-8	1.6	-1.8	14	1.1	4463	12.4	
MWR 14-3-9	1.5	-1.6	15				
MWR 14-3-10	1.5	-1.2	16				
MWR 14-3-11	1.6	-1.4	21				
MWR 14-3-12	-3.4	-10.4	23	0.4	9072	79.9	
MWR 14-3-13	-5.2	-10.5	25				

Note: Concentrations were measured using Q-ICPMS. External reproducibility for Ca and other trace element measurements were < 6% at 2σ level based on repeated analysis of USGS Carbonatite standard COQ-1.

Table 3.4: Geochemical data for samples from siliciclastic and volcaniclastic formations, and silicate fractions in limestones of the Marwar Supergroup

	Sonia Formation						
Sample ID	MWR 14-1	MWR 14-126	MWR 14-127	MWR 14-129	MWR 14-131	MWR 14-132	MWR 14-133
Sc	0.54	9.9	2.0	0.53	1.3	1.3	1.2
V	8.7	59	24	3.1	3.8	4.6	3.4
Cr	135	99	217	149	160	187	152
Co	0.22	4.7	1.2	0.35	0.11	0.10	0.13
Ni	0.47	16.7	5.1	0.37	0.08	0.55	-
Rb	35	136	30	0.44	0.38	1.19	0.73
Sr	21	406	81	25	41	43	48
Y	2.24	26	9.2	1.9	4.1	3.7	3.9
Zr	50	212	77	23	51	42	53
Nb	0.83	11.4	4.8	0.46	1.9	1.5	1.7
Cs	0.59	14	2.3	0.09	0.06	0.10	0.08
Ba	267	250	82	6.3	17	30	20
La	4.1	35.7	12.6	6.0	9.1	9.3	10.8
Ce	8.1	75	27.8	12.3	19.4	20.4	24.2
Pr	0.91	8.7	2.99	1.32	2.14	2.19	2.57
Nd	3.3	32.0	11.6	4.7	7.6	7.8	8.8
Sm	0.59	6.6	2.66	0.72	1.23	1.36	1.38
Eu	0.21	1.20	0.47	0.157	0.32	0.34	0.37
Gd	0.59	6.9	2.23	0.72	1.21	1.32	1.39
Tb	0.072	0.87	0.275	0.075	0.141	0.141	0.154
Dy	0.38	4.70	1.71	0.39	0.81	0.81	0.82
Ho	0.073	0.92	0.37	0.073	0.160	0.143	0.152
Er	0.231	2.59	1.13	0.234	0.49	0.47	0.44
Tm	0.034	0.39	0.163	0.037	0.076	0.069	0.069
Yb	0.262	2.59	1.07	0.279	0.56	0.51	0.52
Lu	0.038	0.38	0.160	0.039	0.088	0.078	0.081
Hf	1.3	5.9	2.2	0.68	1.4	1.14	1.5
Ta	0.061	0.90	0.43	0.023	0.13	0.111	0.13

Pb	4.5	6.8	1.5	2.2	1.8	1.9	2.4
Th	1.9	16	7.7	2.9	4.0	3.5	3.9
U	0.41	2.1	0.98	0.27	0.35	0.29	0.35
Th/Sc	3.6	1.6	3.8	5.5	3.0	2.6	3.2
Zr/Sc	93	21	39	44	39	32	44
La_N/Yb_N	11.1	9.9	8.5	15.5	11.6	13.0	14.9
Gd_N/Yb_N	1.86	2.2	1.72	2.12	1.78	2.12	2.20
Eu/Eu*	1.08	0.5	0.59	0.67	0.81	0.78	0.81
$^{143}Nd/^{144}Nd$	0.511537	0.511817	0.511833	0.511805	0.511777	0.511746	0.511728
ε_{Nd} (0)	-21.5	-16.0	-15.7	-16.3	-16.8	-17.4	-17.8
$f^{Sm/Nd}$	-0.42	-0.38	-0.29	-0.52	-0.50	-0.49	-0.52
T_{DM} (Ga)	2.4	2.2	2.6	1.7	1.8	1.9	1.8
$^{87}Sr/^{86}Sr$	0.792722	0.721773	0.721611	0.714306	0.713373	0.714099	0.713215

	Sonia Formation						
Sample ID	MR 14-1	MR 14-2	MR 14-13	MR 14-15	MR 14-17	MWR 15-1	MWR 15-2
Sc	10.72	1.0	3.9	0.70	0.42	0.58	0.88
V	61.92	5.8	27	5.5	5.3	5.3	10.8
Cr	90	109	175	144	156	140	252
Co	9.7	0.39	2.3	0.22	0.30	0.10	0.73
Ni	24	0.28	4.7	0.45	-	0.67	2.8
Rb	159	31	90	2.8	2.1	2.1	6.1
Sr	43	14	40	7.1	32	15	9.3
Y	11.00	2.4	8.5	6.9	3.0	1.6	3.1
Zr	127	48	108	56	32	76	30
Nb	11.8	1.7	5.5	2.0	0.76	1.8	2.2
Cs	13.86	1.2	6.4	0.24	0.13	0.08	0.33
Ba	408	98	283	17	7.3	3.9	23
La	22.4	9.3	12.2	7.1	8.7	5.2	13.0
Ce	45	18.1	26.3	16.5	17.9	9.0	19.8
Pr	5.16	2.09	2.61	1.62	1.95	1.06	2.33
Nd	18.5	7.2	9.5	5.6	6.4	3.7	8.2
Sm	3.13	1.13	1.94	1.11	0.95	0.73	1.16
Eu	0.66	0.19	0.41	0.21	0.165	0.104	0.165
Gd	3.03	1.06	1.94	1.26	0.99	0.90	1.57
Tb	0.38	0.105	0.251	0.180	0.103	0.069	0.125
Dy	2.13	0.50	1.46	1.20	0.58	0.281	0.52
Ho	0.39	0.092	0.292	0.246	0.115	0.057	0.104
Er	1.17	0.245	0.95	0.76	0.35	0.208	0.35
Tm	0.20	0.038	0.155	0.115	0.054	0.033	0.048
Yb	1.23	0.251	1.09	0.82	0.40	0.263	0.310
Lu	0.184	0.041	0.158	0.118	0.055	0.044	0.047
Hf	3.6	1.3	2.9	1.6	0.92	1.9	0.77
Ta	0.84	0.112	0.39	0.15	0.039	0.108	0.17
Pb	5.79	1.6	4.0	2.9	1.23	1.6	1.9
Th	9.6	2.3	2.9	3.3	2.2	1.9	1.9

U	1.9	0.54	0.63	0.65	0.28	0.46	0.55
Th/Sc	0.90	2.3	0.8	4.6	5.1	3.2	2.1
Zr/Sc	12	48	28	80	75	132	34
La_N/Yb_N	13.0	26.7	8.1	6.2	15.4	14.1	30.1
Gd_N/Yb_N	2.03	3.49	1.48	1.27	2.02	2.82	4.20
Eu/Eu*	0.65	0.53	0.65	0.54	0.52	0.39	0.37
$^{143}Nd/^{144}Nd$	0.511682	0.511636	0.512204	0.511654	0.512152	0.511547	0.511608
ε_{Nd} (0)	-18.7	-19.6	-8.5	-19.2	-9.5	-21.3	-20.1
$f^{Sm/Nd}$	-0.48	-0.52	-0.41	-0.51	-0.55	-0.39	-0.57
T_{DM} (Ga)	2.0	1.9	1.5	1.9	1.2	2.5	1.8
$^{87}Sr/^{86}Sr$	0.840507	0.792406	0.784703	0.712737	0.714125	0.717261	0.738110

	Sonia Formation	Girbhakar Formation		Gotan Formation			
Sample ID	MWR 15-6	MWR 14-128	MR 14-5	MWR 14-40*	MWR 14-66*	MWR 14-86*	MWR 14-95*
Sc	7.2	0.96	0.97	8.1	2.3	2.3	1.15
V	64	9.4	7.1	80	63	75	49
Cr	151	263	197	261	213	267	226
Co	18.9	0.22	0.49	6.9	1.8	5.2	1.6
Ni	35	0.88	1.9	32	13	75	16
Rb	85	2.2	7.9	111	22	20	12.1
Sr	18	60	14	19	12.1	9.2	6.9
Y	13	3.0	2.6	6.1	2.1	3.4	0.63
Zr	120	64	49	149	53	931	23
Nb	9.6	1.8	1.4	13	4.1	4.3	2.3
Cs	5.8	0.05	0.58	8.3	1.9	1.4	0.84
Ba	230	20	16	307	86	123	56
La	28.5	13.2	8.8	4.2	1.17	0.64	0.22
Ce	55	25.1	16.4	8.9	2.61	2.46	0.44
Pr	4.8	2.71	1.97	0.98	0.26	0.148	0.046
Nd	14.7	9.0	6.9	3.7	0.98	0.64	0.17
Sm	2.23	1.45	1.20	0.79	0.23	0.152	0.036
Eu	0.45	0.24	0.158	0.29	0.081	0.078	0.028
Gd	3.5	1.45	0.99	0.96	0.27	0.19	0.048
Tb	0.34	0.150	0.094	0.133	0.043	0.043	0.0090
Dy	1.82	0.67	0.46	0.94	0.290	0.39	0.080
Ho	0.38	0.116	0.089	0.209	0.060	0.098	0.018
Er	1.19	0.35	0.269	0.68	0.187	0.35	0.061
Tm	0.184	0.049	0.037	0.120	0.032	0.064	0.0110
Yb	1.20	0.35	0.271	0.80	0.222	0.44	0.075
Lu	0.180	0.052	0.042	0.122	0.031	0.074	0.0120
Hf	2.3	1.8	1.3	3.1	0.88	15	0.42
Ta	0.75	0.105	0.070	0.94	0.32	0.31	0.16
Pb	11.8	2.0	0.58	31	5.0	5.7	1.5
Th	10.6	6.0	2.7	5.8	1.3	0.88	0.38
U	3.1	0.36	0.44	20	6.4	11.6	4.5

Th/Sc	1.5	6.3	2.8	0.7	0.5	0.4	0.33
Zr/Sc	17	66	50	18	23	413	20
La_N/Yb_N	17.0	27.4	23.3	3.8	3.78	1.03	2.06
Gd_N/Yb_N	2.4	3.47	3.03	0.99	0.99	0.36	0.529
Eu/Eu*	0.5	0.51	0.44	1.02	1.01	1.39	2.06
$^{143}Nd/^{144}Nd$	0.511521	0.511614	0.511519	0.511747	0.511760	0.511861	0.511950
ε_{Nd} (0)	-21.8	-20.0	-21.8	-17.4	-17.1	-15.2	-13.4
$f^{Sm/Nd}$	-0.54	-0.52	-0.55	-0.35	-0.29	-0.28	-0.36
T_{DM} (Ga)	2.0	1.9	1.9	2.5	2.8	2.7	2.1
$^{87}Sr/^{86}Sr$	0.874059	0.715586	0.729132				

	Nagaur Formation				Tunklian Formation		
Sample ID	MWR 14-13	MWR 14-14	MWR 14-15	MR 14-11	MWR 14-45	MWR 14-46	MR 14-8
Sc	6.0	1.4	1.4	3.5	3.2	1.11	1.3
V	19	7.8	14	21	28	5.8	6.5
Cr	124	201	99	174	70	182	130
Co	2.4	0.35	0.34	0.49	2.7	0.21	1.3
Ni	14	0.93	0.020	0.60	5.6	0.33	1.6
Rb	150	7.4	0.44	60	60	4.3	4.9
Sr	40	5.9	83	25	17	8.4	6.0
Y	8.5	13	5.4	16	9.4	12.0	12.3
Zr	75	117	95	196	160	72	86
Nb	5.1	5.4	2.2	5.6	8.5	2.4	3.3
Cs	8.3	0.65	0.04	1.1	3.9	0.29	0.40
Ba	457	24	16	387	186	23	24
La	7.7	11.0	13.2	12.6	19.0	9.0	9.2
Ce	13.6	19.7	31.1	24.8	37	17.6	21.3
Pr	1.43	2.04	3.6	3.13	3.7	2.42	2.57
Nd	5.1	7.2	13.6	11.5	13.0	8.8	10.0
Sm	1.14	1.52	2.03	2.36	2.30	1.80	2.49
Eu	0.38	0.26	0.37	0.51	0.38	0.35	0.47
Gd	1.23	1.83	1.82	2.53	2.19	2.03	2.48
Tb	0.206	0.298	0.196	0.41	0.243	0.317	0.36
Dy	1.33	2.04	1.02	2.65	1.45	2.09	2.20
Ho	0.287	0.43	0.218	0.55	0.303	0.43	0.42
Er	0.87	1.31	0.67	1.67	1.04	1.31	1.25
Tm	0.137	0.213	0.114	0.257	0.169	0.202	0.181
Yb	0.98	1.42	0.82	1.819	1.229	1.392	1.309
Lu	0.140	0.209	0.131	0.266	0.184	0.202	0.187
Hf	2.1	3.4	2.6	5.4	4.3	2.0	2.4
Ta	0.42	0.44	0.18	0.42	0.66	0.21	0.25
Pb	11.3	4.1	4.6	5.1	4.8	3.6	6.0
Th	5.2	6.3	6.7	7.4	5.9	5.1	11.5
U	0.74	1.05	0.68	1.7	1.5	0.74	0.96
Th/Sc	0.9	4.6	4.8	2.1	1.8	4.6	8.8
Zr/Sc	13	86	68	55	50	65	66

La_N/Yb_N	5.7	5.5	11.6	5.0	11.1	4.7	5.1
Gd_N/Yb_N	1.04	1.06	1.84	1.15	1.48	1.20	1.57
Eu/Eu*	0.98	0.48	0.60	0.64	0.52	0.55	0.58
$^{143}Nd/^{144}Nd$	0.511797	0.511879	0.511887	0.511531	0.511605	0.511999	0.511936
ε_{Nd} (0)	-16.4	-14.8	-14.7	-21.6	-20.2	-12.5	-13.7
$f^{Sm/Nd}$	-0.32	-0.35	-0.41	-0.38	-0.45	-0.34	-0.25
T_{DM} (Ga)	2.5	2.2	2.0	2.6	2.2	2.0	2.7
$^{87}Sr/^{86}Sr$	0.813217	0.747717	0.725610	0.809584	0.844489	0.733829	0.737797

	Chhoti Khatu Tuff					
Sample ID	MWR 15-3	MWR 15-4	MWR 15-5	MWR 15-7	MWR 15-8	MWR 15-9
Sc	5.8	5.4	5.5	4.8	4.3	3.7
V	52	45	71	87	46	32
Cr	89	99	107	86	131	93
Co	23	20	10.3	10.4	15	11.9
Ni	26	21	33	32	13.0	18
Rb	90	84	79	65	57	55
Sr	18	18	12.8	10.6	11.4	9.4
Y	11.1	10.9	11.4	10.5	11.6	7.0
Zr	137	163	132	113	157	90
Nb	9.6	10.9	9.4	9.3	9.9	7.6
Cs	7.1	6.5	5.5	4.4	4.0	6.3
Ba	205	200	195	163	150	125
La	13.5	21.8	15.9	12.7	19.6	11.3
Ce	38	41	32	24.8	36	19.8
Pr	3.7	4.0	3.24	2.48	3.6	1.86
Nd	12.3	13.4	11.3	8.7	12.2	6.3
Sm	2.20	2.43	2.06	1.61	2.34	1.18
Eu	0.41	0.42	0.39	0.31	0.399	0.229
Gd	2.22	2.35	2.18	1.69	2.36	1.21
Tb	0.279	0.287	0.277	0.235	0.306	0.154
Dy	1.74	1.71	1.72	1.52	1.87	1.02
Ho	0.38	0.37	0.38	0.34	0.389	0.237
Er	1.25	1.24	1.23	1.14	1.22	0.79
Tm	0.207	0.202	0.195	0.183	0.202	0.129
Yb	1.47	1.43	1.40	1.26	1.37	0.96
Lu	0.222	0.219	0.205	0.193	0.206	0.146
Hf	3.7	4.3	3.4	2.9	4.1	2.3
Ta	0.80	0.87	0.73	0.78	0.79	0.60
Pb	5.2	4.9	4.5	3.3	4.7	2.9
Th	7.2	7.8	6.5	4.9	6.6	4.2
U	4.2	3.7	3.7	3.7	3.5	2.8
Th/Sc	1.2	1.5	1.2	1.0	1.5	1.1
Zr/Sc	23	31	24	24	36	25
La_N/Yb_N	6.6	10.9	8.2	7.3	10.2	8.5
Gd_N/Yb_N	1.25	1.36	1.29	1.11	1.42	1.04

Eu/Eu*	0.57	0.54	0.57	0.58	0.52	0.59
$^{143}Nd/^{144}Nd$	0.511599	0.511567	0.511563	0.511558	0.511601	0.511581
ε_{Nd} (0)	-20.3	-20.9	-21.0	-21.1	-20.2	-20.6
$f^{Sm/Nd}$	-0.45	-0.45	-0.44	-0.43	-0.41	-0.43
T_{DM} (Ga)	2.2	2.3	2.3	2.3	2.4	2.3
$^{87}Sr/^{86}Sr$	0.904225	0.899269	0.941002	0.944467	0.909963	0.921283

Note: * indicates only silicate fraction of the limestone is analysed for trace element concentration. Concentrations are in ppm. External reproducibility of trace element contents is <8% and that of REE's is <3% at 2σ level based on the repeated analysis of BHVO-2. Subscript N indicates concentrations are normalized with Chondritic values. $Eu/Eu^* = Eu_N/(Sm_N \times Gd_N)^{0.5}$. $\varepsilon_{Nd}(0) = [(^{143}Nd/^{144}Nd_{sample}/^{143}Nd/^{144}Nd_{CHUR}) - 1] \times 10^4$ and was calculated using present day CHUR value of $^{143}Nd/^{144}Nd = 0.512638$. $f^{Sm/Nd}$ is calculated using present day CHUR value of $^{147}Sm/^{144}Nd = 0.1967$. Depleted Mantle Nd model age (T_{DM}) is calculated using Depleted Mantle reservoir ratios of $^{143}Nd/^{144}Nd = 0.51315$ and $^{147}Sm/^{144}Nd = 0.2137$.

Table 3.5: Geochemical data for samples from the basement rocks of Marwar Basin

	Malani Igneous Suite			Erinpura Granites			Delhi Supergroup
Sample ID	MWR 14-130	MR 14-14	MWR 14-134	ERG	Sirohi 14-1	Sirohi 14-2	PH 15-1
Sc	1.01	8.4	1.12	9.1	13	8.6	6.0
V	5.2	3.5	2.2	20	70	15	41
Cr	166	67	158	188	292	300	79
Co	1.17	0.67	0.69	4.4	12.0	0.65	8.7
Ni	3.9	1.06	2.5	7.2	21	5.1	25
Rb	142	133	188	214	277	1.3	0.71
Sr	8.4	31	6.3	135	60	388	131
Y	135	59	159	51	46	53	22
Zr	1187	540	1263	149	85	58	90
Nb	26	17	27	17	19	11.2	7.6
Cs	2.8	4.0	7.9	4.7	21	0.21	0.089
Ba	71	653	139	1288	396	72	8.1
La	70	53	23.1	74	63	18.4	5.4
Ce	164	126	145	155	132	39	17.8
Pr	22.8	17.4	8.8	18.2	14.6	4.9	2.83
Nd	92	73	42	69	53	20.3	12.4
Sm	22.2	16.3	18.5	13.5	10.5	5.8	3.24
Eu	1.10	2.69	1.08	2.54	1.24	1.04	0.75
Gd	22.7	14.6	21.1	12.2	10.5	6.6	3.4
Tb	3.6	1.96	3.8	1.67	1.44	1.21	0.57
Dy	23.4	11.4	25.9	9.6	8.4	8.4	3.6
Ho	4.9	2.31	5.4	1.81	1.67	1.90	0.74
Er	14.4	7.0	16.1	5.2	4.9	5.8	2.11
Tm	2.16	1.00	2.42	0.75	0.71	0.90	0.315
Yb	14.5	7.2	16.0	4.9	4.6	5.8	2.09
Lu	2.04	1.02	2.32	0.69	0.65	0.74	0.304
Hf	26	14	29	5.0	2.4	1.7	2.6

Ta	1.5	1.10	1.6	1.3	1.5	0.96	0.64
Pb	7.0	11.1	10.4	39	23	7.0	4.2
Th	14	9.2	15	32	40	29	3.4
U	3.3	1.7	3.0	3.5	2.7	3.5	2.0
Gd_N/Yb_N	1.3	1.7	1.1	2.1	1.9	0.9	1.4
$^{143}Nd/^{144}Nd$	0.512638	0.512655	0.512985	0.512105	0.511814	0.512061	0.512047
ε_{Nd} (0)	0.0	0.3	6.8	-10.4	-16.1	-11.3	-11.5
$f^{Sm/Nd}$							
T_{DM} (Ga)	1.0	0.9		1.6	2.1		2.9
$^{87}Sr/^{86}Sr$	1.158436	0.808594	1.367432	0.760482	0.856725	0.720317	0.718082

	Delhi Supergroup					Banded Gneissic Complex-2	
Sample ID	PH 15-2	PH 15-45	PH 15-28	PH 15-16	PH 15-30	PH 15-34	PH 15-36
Sc	3.8	12.1	3.2	14	14	15	2.0
V	3.9	21	0.82	80	76	84	8.2
Cr	98	40	44	185	235	147	91
Co	0.76	3.6	0.009	17	9.3	13	5.6
Ni	1.5	6.7	1.3	32	10.9	13	5.3
Rb	85	3.2	280	126	117	150	93
Sr	46	32	97	58	19	199	223
Y	2.1	3.7	0.041	21	25	58	3.6
Zr	22	11.1	0.18	122	96	9.8	29
Nb	10.8	2.2	0.06	16.7	17.8	22.7	2.5
Cs	6.4	0.26	11.2	5.4	4.4	0.92	0.73
Ba	37	9.4	331	514	354	1103	2832
La	4.2	1.16	0.225	48	51	115	5.8
Ce	7.1	3.06	0.129	102	110	243	8.2
Pr	0.74	0.39	0.018	11.6	12.2	28.3	1.23
Nd	2.32	1.66	0.056	42	45	107	4.5
Sm	0.48	0.47	0.0126	7.9	8.5	19.3	0.83
Eu	0.260	0.130	0.61	1.54	0.97	2.70	0.84
Gd	0.44	0.52	0.0106	7.5	7.8	17.8	0.81
Tb	0.064	0.093	0.00082	0.90	0.98	2.24	0.098
Dy	0.36	0.61	0.0074	4.6	5.3	11.8	0.53
Ho	0.070	0.124	0.00043	0.80	1.02	2.18	0.113
Er	0.231	0.35	0.0024	2.20	3.11	5.8	0.34
Tm	0.044	0.053	0.00049	0.312	0.50	0.75	0.052
Yb	0.36	0.37	0.0036	2.11	3.7	4.5	0.40
Lu	0.059	0.052	0.00037	0.308	0.56	0.61	0.070
Hf	0.79	0.32	0.0057	3.3	2.6	0.44	1.07
Ta	1.00	0.64	0.033	1.09	1.3	1.02	0.60
Pb	23	1.3	110	16	7.0	24	11.8
Th	1.5	0.21	-	23	26	20	14
U	0.39	0.26	0.056	2.1	3.1	1.5	6.5
Gd_N/Yb_N	1.03	1.17	2.46	2.9	1.7	3.2	1.68

$^{143}Nd/^{144}Nd$	0.511900	0.511738		0.511835	0.511765	0.511230	0.511101
ε_{Nd} (0)	-14.4	-17.6		-15.7	-17.0	-27.5	-30.0
$f^{Sm/Nd}$							
T_{DM} (Ga)	2.1					2.7	2.9
$^{87}Sr/^{86}Sr$	0.797128	0.729322	0.826255	0.798371	0.899851	0.758792	0.736112

	Banded Gneissic Complex-2	
Sample ID	PH 15-37	PH 15-38
Sc	4.9	14
V	24	49
Cr	117	106
Co	5.2	7.4
Ni	7.2	10.5
Rb	106	82
Sr	193	113
Y	19	44
Zr	187	66
Nb	6.1	14
Cs	1.09	1.16
Ba	509	422
La	37	87
Ce	88	164
Pr	9.7	18.8
Nd	36	67
Sm	8.0	12.2
Eu	1.38	1.90
Gd	7.2	12.1
Tb	0.86	1.56
Dy	4.1	8.8
Ho	0.68	1.649
Er	1.77	4.5
Tm	0.236	0.62
Yb	1.52	3.8
Lu	0.220	0.52
Hf	5.5	2.3
Ta	0.51	1.01
Pb	36	18
Th	25	28
U	2.1	1.7
Gd_N/Yb_N	3.9	2.6
$^{143}Nd/^{144}Nd$	0.511750	0.511334
ε_{Nd} (0)	-17.3	-25.4
$f^{Sm/Nd}$		
T_{DM} (Ga)	2.6	2.6

$^{87}Sr/^{86}Sr$	0.753648	0.776734

Note: Experimental details as mentioned in Table 3.4.